

Active Galactic Nuclei – the Physics of Individual Sources and the Cosmic History of Formation and Evolution

Henric Krawczynski¹ and Ezequiel Treister²

¹ Washington University in St. Louis

² Universidad de Concepción, Departamento de Astronomía,
Casilla 160-C, Concepción, Chile

Correspondence: Henric Krawczynski (krawcz@wuphys.wustl.edu) and
Ezequiel Treister (etreiste@astro-udec.cl)

January 18, 2013

Abstract

In this paper we give a brief review of the astrophysics of active galactic nuclei (AGN). After a general introduction motivating the study of AGNs, we discuss our present understanding of the inner workings of the central engines, most likely accreting black holes with masses between 10^6 and $10^{10} M_{\odot}$. We highlight recent results concerning the jets (collimated outflows) of AGNs derived from X-ray observations (Chandra) of kpc-scale jets and γ -ray observations of AGNs (Fermi, Cherenkov telescopes) with jets closely aligned with the lines of sight (blazars), and discuss the interpretation of these observations. Subsequently, we summarize our knowledge about the cosmic history of AGN formation and evolution. We conclude with a description of upcoming observational opportunities.

1 Motivation

Active galactic nuclei (AGNs) are galaxies that harbor supermassive black holes (SMBHs) of a few million to a few billion solar masses. Whereas it seems likely that all galaxies contain one or more supermassive black holes [1, 2], the black holes in AGNs give rise to spectacular observational consequences because they accrete matter and convert the gravitational energy of the accreted matter (and possibly also the rotational energy of the black hole) into mechanical and electromagnetic energy. A few of the most salient motivations for the study of AGNs are:

AGN Taxonomy: AGNs are among the brightest extragalactic sources and account for a large fraction of the electromagnetic energy output of the Universe, motivating their taxonomy

and statistical characterization. The study of AGNs in the nearby Universe shows that the diversity of AGNs can be understood as resulting from observing a smaller number of basic AGN types from different viewing angles (see Section 3.1).

Accretion Physics: AGNs are powered by the accretion of magnetized plasma. Studies of AGN accretion flows complement studies of other accretion flows in astrophysics: accretion onto protostars and stars, accretion onto compact stellar remnants (neutron stars and stellar mass black holes), and the accretion that powers gamma-ray bursts. One goal of the studies of AGN accretion flows is to provide a physical explanation of the different types of AGNs and their states in terms of the nature of their accretion flows and environments (see Section 3.3).

Role in Eco-Systems: AGNs play an important role for galactic and galaxy cluster eco-systems, i.e. their mechanical and electromagnetic power contributes to the heating of the interstellar and intracluster medium, and thus influences the star formation of the host systems (see Section 2.4).

History through Cosmic Time: Deep radio, IR, optical and X-ray observations of AGNs have provided us with a wealth of information about the cosmic history of the formation and growth of supermassive black holes and the evolution of AGNs. Related areas of research are to clarify the role of AGNs in re-ionizing the intergalactic medium, and to explain the correlation between black hole masses and the properties of the host galaxy observed in the local Universe (see Sections 4 & 5).

Fundamental Physics: On the most fundamental level, AGNs allow us to test the theory of general relativity (GR). GR's no-hair theorem states that Kerr (and more generally Kerr-Newman) solutions are the only stationary, axially symmetric vacuum solutions of the Einstein equations with an event horizon. Testing if astrophysical black holes are Kerr black holes thus constitutes a powerful test of GR in the observationally poorly constrained strong-gravity regime [3].

Astroparticle Physics: AGNs are astroparticle physics laboratories. A few examples: The TeV γ -ray emission from AGNs tells us that they can accelerate particles to $> \text{TeV}$ energies and AGNs might even be the sources of Ultra High Energy Cosmic Rays. The studies of the broadband emission from AGNs allows us to perform time resolved studies of the particle acceleration processes. AGN observations can also be used to constrain Lorentz Invariance violations [e.g. 4], and to set upper and lower limits on extragalactic magnetic fields (see the discussion in [5, 6]).

AGNs as Beacons at Cosmological Distances: The emission from AGNs can be used to study the properties of objects, diffuse matter, and radiation fields that are located between us and the AGNs. High-resolution spectra of high-redshift, low-metallicity quasar absorption line systems have been used to constrain the relative abundance of the light elements produced during the epoch of the Big Bang Nucleosynthesis [7]. Measurements of the Gunn-Peterson



Figure 1: Comparison of the morphologies of a FRI radio galaxy (M84, left panel) and a FRII radio galaxy (3C 175, right panel). M84 is a massive elliptical galaxy in the Virgo cluster. The false-color composite image shows the Very Large Array 4.9 GHz image of the radio galaxy in red [11], the Chandra 0.5-2 keV image of hot galaxy gas in blue [12], and a Sloan Digital Sky Survey optical image in yellow and white. The radio galaxy has a projected diameter of ≈ 12 kpc. The Very Large Array 4.9 GHz image of 3C 175 ($z = 0.768$) shows a well-collimated jet, and two hot spot complexes typical for FRII radio galaxies. The projected distance between the two hotspots at the two ends of the radio galaxy is ≈ 370 kpc. Credits for the left panel: X-ray (NASA/CXC/MPE/A.Finoguenov et al.); Radio (NSF/NRAO/VLA/ESO/R.A.Laing et al); Optical (SDSS). The right image is a courtesy of NRAO/AUI.

optical depths of high-redshift quasars constrain the re-ionization history of the intergalactic medium [8]. X-Ray Absorption lines constrain the abundance and properties of warm-hot intergalactic medium [9]. The study of the GeV and TeV γ -ray energy spectra of blazars can be used to constrain the energy spectrum of the infrared and optical Extragalactic Background Light [10].

The discussion in this paper is limited to recent results concerning the properties and inner workings of AGNs, and does not cover the research that uses AGNs as probes of the intervening medium. In Sect. 2 we discuss observations of AGN jets and their interpretation. In Sect. 3 we describe observations of the AGN cores, as well as models of AGN accretion and jet formation. We review recent results concerning the cosmic history of black hole accretion in Sect. 4, and trigger of black hole growth in Sect. 5. We conclude with a brief description of upcoming observational opportunities afforded by present and upcoming experiments in Sect. 6.

2 AGN Jets on pc, kpc and Mpc Scales

2.1 Morphology of Radio Galaxies

Some of the gravitational energy of the material accreted by AGNs is converted into heat and electromagnetic radiation inside the accretion disk and is radiated away by the accretion disk. Some of the material processed through the accretion disk escapes the accretion system as collimated (jets) and uncollimated (winds) outflows. The event horizon of a non-rotating Schwarzschild black hole is two times the gravitational radius:

$$r_g = \frac{GM_{\text{BH}}}{c^2} \approx 1.48 \frac{M_{\text{BH}}}{10^8 M_{\odot}} 10^{13} \text{ cm} \quad (1)$$

Approximately 10%-20% of AGNs are radio loud (radio to optical spectral index >0.35 , see e.g. [13, 14]), and show bright extended radio features with sizes up to ~ 1 Mpc (3.08×10^{24} cm). The AGN phenomenon thus spans ~ 11 orders of magnitudes in size scales.

The first jet of a SMBH was observed in the optical: in 1918, H. D. Curtis wrote about the object M 87 in the Virgo cluster [17]: “A curious straight ray lies in a gap in the nebulosity in p.a. 20° , apparently connected with the nucleus by a thin line of matter.” It was not before 1963 that the extragalactic nature of quasars (quasi-stellar objects, a type of AGNs) was established when Schmidt measured the redshift $z = 0.158$ of the radio source 3C 273 [18]. We now know that radio-loud galaxies come in two qualitatively different types (see Fig. 1): Fanaroff-Riley Class I (FRI) sources have center-brightened outflows and Fanaroff-Riley Class II (FRII) exhibit an edge-brightened morphology. Whereas the separation of the regions of highest radio brightness of FRI sources are smaller than half the size of the radio source, those of FRII sources are larger than half the size of the radio source. FRI sources are less powerful than FRII sources, with 1.4 GHz luminosities below and above $5 \times 10^{25} \text{ W Hz}^{-1}$, respectively.

The observations of AGNs with single-dish and interferometric radio telescopes and with optical telescopes have provided us with detailed information about the morphology of radio-loud AGNs. As an example, Fig. 2 shows radio and optical images of M 87 with various resolutions, zooming in from an image of radio lobes blown by the central engine into the intracluster gas to the inner jet imaged with a resolution of a few $10 r_g$. One distinguishes between the unresolved radio-core (which is likely to coincide with the location of the SMBH), the well collimated jet (which transports energy away from the SMBH), jet knots (locations of increased energy dissipation), hotspots and hotspots complexes (where the jet impinges on the ambient medium and most of the mechanical jet energy is dissipated in strong shocks), and lobes of radio-emitting plasma.

Radio-interferometric (and sometimes optical) observations of some AGNs reveal jet features moving with apparent motions exceeding the speed of light. Such “superluminal” motion can be explained by a near-alignment of the jet with the line of sight combined with highly-relativistic motion of the radio plasma. Photons emitted over a certain time interval reach the observer in a shortened time span as the plasma travels almost with the speed of light and thus stays closely behind photons emitted towards the observer. The apparent velocity can then exceed the speed of light.

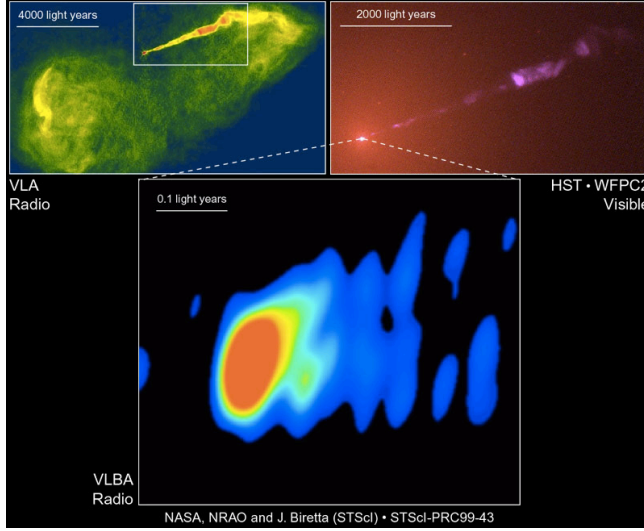


Figure 2: Images of the radio galaxy M87 at the center of the Virgo galaxy cluster at different spatial scales and in different wavelengths. The Very Large Array radio image (top left) side shows the kpc-scale jet inflating radio lobes. The Hubble Space Telescope optical image (top right) shows the structure of the kpc-scale jet. The Very Long Baseline Array image (bottom center) shows the sub-pc scale jet very close to the black hole. Credits: National Radio Astronomy Observatory/National Science Foundation, NASA and John Biretta (STScI/JHU), National Radio Astronomy Observatory/Associated Universities, Inc.

If we denote the jet plasma velocity with $v = \beta_j c \approx c$ (c being the speed of light), we can introduce the bulk Lorentz factor of the plasma with

$$\Gamma_j = (1 - \beta_j^2)^{-1/2}. \quad (2)$$

Emission from the jets is red or blue-shifted by the relativistic Doppler factor

$$\delta_j = \frac{1}{\Gamma_j(1 - \beta_j \cos \theta)} \quad (3)$$

with θ being the angle between the jet axis and the line of sight as measured in the observer frame. A detailed study of a statistically complete, flux-density-limited sample of 135 compact radio sources with the Very Long Baseline Array (VLBA) and the Metsähovi Radio Observatory reveals relativistic motion with bulk Lorentz factors Γ_j between 1 and ~ 40 [20].

2.2 X-ray and Gamma-Ray Observations of kpc-Scale Jets

The Chandra X-ray observatory discovered X-ray emission from the kpc-scale jets and hotspots of a large number of radio-loud AGNs [21]. The XJET web-site¹ lists the detection of X-ray emission associated with the jets from ~ 120 AGNs. The origin of the X-ray emission is still somewhat uncertain, especially for the higher-power FRII-type sources.

For the low-power FRI-type sources, the X-ray emission from the kpc-jets can in most cases be explained as synchrotron emission from $\sim \text{TeV}$ electrons gyrating in 10-1000 μG magnetic fields. As electrons lose their energy on time scales of years, the X-ray bright spots imply in-situ particle acceleration. Well resolved jets show X-ray bright knots, sometimes spread over the extension of the jet (Fig. 3). The hypothesis of a synchrotron origin of the X-rays is supported by the rapid time variability of the X-ray flux from the knots of the M87 jet [21], the radio to X-ray energy spectra which allow modeling with a single synchrotron component with a monotonic softening of the energy spectrum from the radio to the X-ray band (Fig. 4, left panel), and the relative morphologies of the radio, optical and X-ray emission.

For the higher-power FRII-type sources, the radio to X-ray energy spectrum can often not be described with a single synchrotron component as the radio, optical and X-ray observations imply a significant hardening of the energy spectrum between the optical and the X-ray band (Fig. 4, right panel). The presently favored explanation of the X-ray emission is that it originates as inverse-Compton emission of mildly relativistic ($\sim \text{MeV}$) electrons embedded in a highly relativistic plasma moving with a bulk Lorentz factor $\Gamma \sim 10$. In the co-moving reference frame of the jet plasma (primed variables), the mean frequency of cosmic microwave background (CMB) photons is

$$\nu'_{\text{CMB}} = (1 + z) \Gamma_j \nu_0 \quad (4)$$

and the CMB energy density is

$$u'_{\text{CMB}} \approx (1 + z)^4 \Gamma_j^2 u_{\text{CMB},0} \quad (5)$$

with the local present day values $\nu_0 \approx 1.6 \times 10^{11}$ Hz and $u_{\text{CMB},0} \approx 4 \times 10^{-13}$ erg cm^{-3} . The boosting of the mean energy and energy density proportional to Γ_j and Γ_j^2 , respectively, explains the presence of a relatively strong inverse-Compton component in the X-ray band. The inverse-Compton/CMB model predicts an increase of the X-ray to radio brightness proportional to the energy density of the CMB which scales with $(1 + z)^4$. The data indeed show such a trend for a small sample of sources (Fig. 5). However, the model faces several problems: for some of the sources the inverse-Compton/CMB model implies very small viewing angles and thus large physical source diameters on the order of hundreds of Mpc [22]; furthermore, for some jets, the model parameters imply a rather high jet power ($\sim 10^{48}$ erg s^{-1}) [23]. With regards to jet models, the most interesting implication of the inverse-Compton/CMB model is the relativistic motion of the jet plasma at $\sim \text{kpc}$ distances from the SMBH. An alternative explanation for the observed X-ray emission is synchrotron emission from an additional high-energy electron population [22].

¹<http://hea-www.harvard.edu/XJET/>

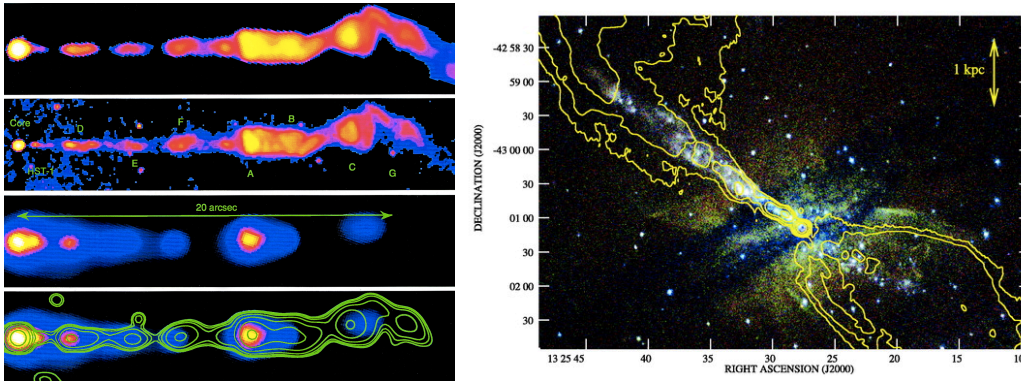


Figure 3: Multiwavelength images of the radio galaxies M87 (left panel) and Cen A (right panel). The left image shows from top to bottom the 14.435 GHz Very Large Array (VLA) image, the Hubble Space Telescope Planetary Camera image in the F814W filter, and the the Chandra X-ray (keV) image; the bottom panel shows the Chandra image overlaid with contours of the Hubble Space Telescope image smoothed to match the Chandra point response function. The Hubble Space Telescope and Very Large Array images use a logarithmic color scale, and the X-ray image uses a linear scale. The portion of the jet shown in the image has a projected length of ≈ 1.6 kpc. The right image shows a false-color image of the radio galaxy Centaurus A as seen by Chandra (color image: 0.4-0.85 keV (red), 0.85-1.3 keV (green), and 1.3-2.5 keV (blue)) and the VLA at 5 GHz (contours at $7 \times (1, 4, 16, \dots)$ mJy beam $^{-1}$). The portion of the northern X-ray jet has a projected length of ≈ 3 kpc. The left panel is reproduced from Ref. [15], ©2002 American Astronomical Society, and the right panel is reproduced from Ref. [16], ©2007 American Astronomical Society.

However, in this case, the peak position of the second emission component at \gg keV-energies remains unexplained.

The Fermi LAT has recently detected emission from the core, and the northern and southern lobes of the radio galaxy Cen A [24, 25]. The emission can be explained as inverse-Compton emission from electrons scattering photons of the CMB and maybe also higher-frequency photons. Whereas the synchrotron radio emission traces the combined properties of the radio-emitting electrons and the magnetic field strength, the inverse-Compton emission in the γ -ray band traces the high-energy electrons more directly. The combined data can also be used to set an upper limit on the magnetic field B in the lobes of $B < 1 \mu\text{G}$. It would be extremely interesting to obtain a γ -ray image with a substantially improved signal-to-noise ratio.

2.3 Composition of AGN Jets

It is quite remarkable that we are still uncertain about the composition of AGN jets. One of the reasons is the dominance of non-thermal continuum emission from jets leading to a lack of detected

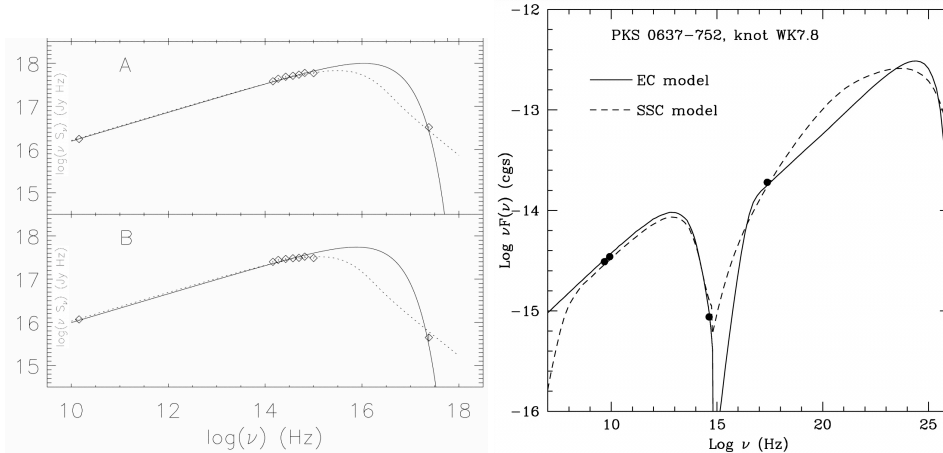


Figure 4: Spectral energy distribution of two knots of the M87 jet (left panel, see the left lower-center panel of Fig. 3 for the labels of the knots). The radio, optical and X-ray flux points can be explained with a single population of non-thermal electrons (and/or positrons) with an energy spectrum that softens monotonically with energy. The dashed and dotted lines show synchrotron models. The right panel presents the spectral energy distribution of the knot WK7.8 of the quasar PKS 0637-752 that shows evidence for two emission components, one component extending from radio to X-rays and another one extending from X-rays to gamma-rays. The authors favor the inverse Compton/CMB model (solid line) over the SSC model (dashed line) as the former requires less power than the latter (3×10^{48} ergs s^{-1} compared to $> 10^{49}$ ergs s^{-1}). The left panel is reproduced from Ref. [15], ©2002 American Astronomical Society, and the right panel is reproduced from Ref. [19], ©2000 American Astronomical Society.

lines that give away the nature of the jet plasma. Theoretical considerations suggest that the energy and momentum of the jets is initially (at distances of a few $10 r_g$) dominated by electromagnetic energy (Poynting flux). At larger distances (on the order of a few 100 or 1000 r_g) the electromagnetic energy is transferred to particles. The particles carrying the energy might be electrons and positrons or Interstellar Medium (ISM) processed through the accretion disk and/or entrained along the way. The jet may entrain additional ISM as it propagates, leading to a decrease of Γ_j with distance from the central engine.

For Flat Spectrum Radio Quasars (FSRQs), Sikora & Madejski (2000) argue that jets with $\Gamma_j \sim 10$ cannot be dominated by cold pairs at their bases, as the inverse-Compton emission from the pairs scattering UV-radiation from the accretion disk would give rise to an unobserved soft X-ray emission component [27] (see also [28, 29]).

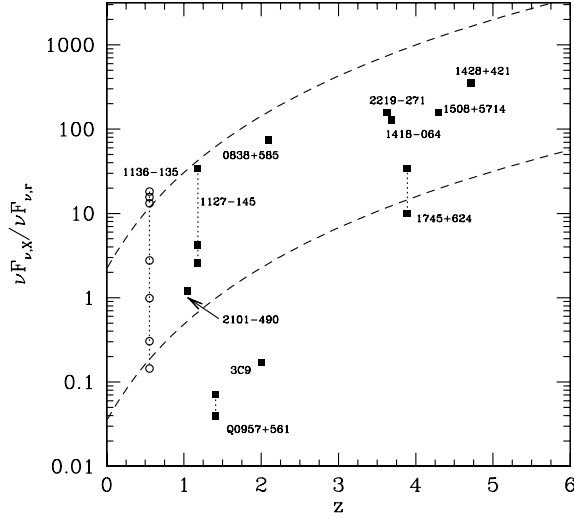


Figure 5: Ratio of the X-ray and radio fluxes of high-redshift ($z > 1$) jets discovered with Chandra following [26]. For the nearby source PKS 1136135 at $z = 0.5$ the spread of the $z < 1$ jet population is shown. The data indicate that the ratio follows approximately the $(1+z)^4$ -behavior predicted by the inverse-Compton/CMB model, albeit with a large spread (Courtesy of C. C. Cheung, 2012).

2.4 AGN Feedback

Several X-ray observatories (first *ROSAT*, later Chandra and *XMM-Newton*) discovered large “cavities” in the hot X-ray bright gas of elliptical galaxies, galaxy groups, and galaxy clusters associated with the radio lobes of AGNs [30, 31] (see also Fig. 6). The cavities are caused by AGNs inflating bubbles of radio plasma which displaces the hot X-ray bright interstellar or intracluster medium. One can use these cavities to constrain the composition of the radio plasma in the cavities. For galaxy clusters, the intracluster medium (ICM) pressure is well constrained by the spectroscopic X-ray images of the ICM. One can estimate the $p dV$ work required to inflate the bubbles. Combining this work with an estimate of the ages of the cavities (assuming they rise at the local sound speed), one can estimate the power required to inflate the bubbles of radio gas. Comparing the latter with the broadband radio power one can estimate the ratio k of the total jet power divided by the power carried by non-thermal electrons responsible for the observed radio emission. Such studies show $k \sim 100$ (Fig. 7) and the presence of “dark” pressure-contributing components (non-thermal low-energy electrons, non-thermal protons, or magnetic field). Although AGN jets seem to have sufficient power to balance the radiative (Bremsstrahlung) cooling of the intracluster gas and to explain the lack of cold gas and freshly formed stars at the centers of galaxy clusters, the role of AGNs in heating the ICM is not well established [33]. The jet power may not be transformed efficiently into ICM heat, and other processes (i.e. efficient heat conduction owing to anisotropic

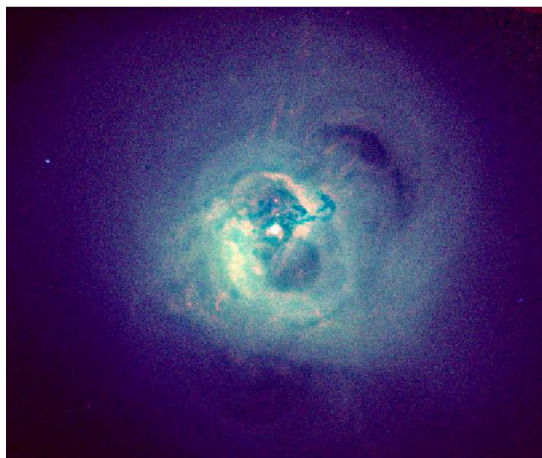


Figure 6: A Chandra X-ray image of the Perseus galaxy cluster showing the emission from the hot ICM. The X-ray brightness clearly shows two cavities carved out by the radio plasma from the central radio galaxy NGC 1275. The ripples in the brightness distribution are explained as the result of sound waves propagating through the ICM. The opposite ends of the two radio bubbles are at a projected distance of ≈ 65 kpc, and the bright ICM emission has a projected diameter of ≈ 360 kpc [from 32]. Credits: NASA/CXC/IoA/A.Fabian et al..

transport properties) may dominate the heating of cluster cores.

2.5 Magnetohydrodynamic Simulations of Jets

The basic theoretical framework that is currently used to explain the observational appearance of radio-galaxies was introduced in the 1970s [35, 36, 37, 38]. However, the predictive power of analytical jet models is limited owing to the non-linear processes taking place as jets propagate through the ambient medium. Recently, it has become possible to study jets with relativistic 3-D hydrodynamic (HD) and magnetohydrodynamic (MHD) codes (see e.g. [39, 40] and references therein). The simulations can reproduce the observed morphologies of radio sources rather well. Combined analytical and numerical studies show that certain ingredients can increase the stability of jets, i.e. magnetic fields, steep pressure gradients, a high density contrast between jet and external medium, fast motion, or sheath/shear velocity outflow around the jet (e.g. [41] and references therein). The codes use the one-fluid approximation and do not model the microscopic effects occurring in the astrophysical plasmas in detail. Particle in cell (PIC) simulations can shed light on some of the processes occurring when relativistic flows propagate through ambient media [e.g. 42].

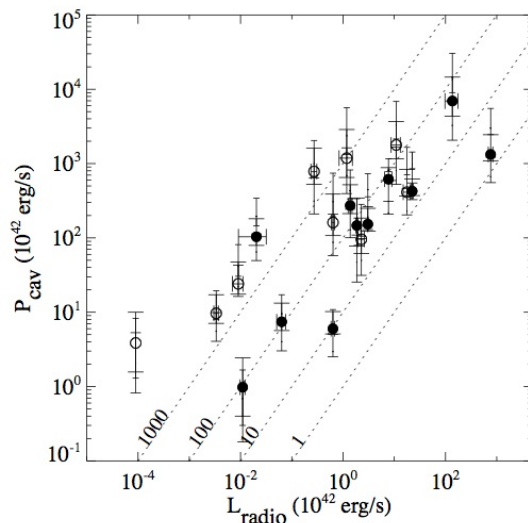


Figure 7: The power required to blow cavities into the ICM as function of the power in the electrons that emit the observed radio emission. The former power exceeds the latter by an average factor on the order of 100 (diagonal lines), indicating that the energy density of the radio plasma in the cavities is dominated by a “dark component” that has not yet been detected. The image is reproduced from Ref. [34], ©2008 American Astronomical Society.

3 Emission from the Central Regions of AGNs

3.1 Overview of Emission Components

The radio, infrared, optical, UV, X-ray and γ -ray observations of AGNs can be explained with a single model of the central AGN region. In the paradigm, the different types of AGN result from different viewing angles towards the symmetry axis, and from the absence or presence of certain components [43]. We briefly explain the most important emission components and their interpretation (see also Fig. 8):

Emission from the Accretion Disk: In some AGNs, emission from the accretion disk itself may have been detected. The feature, often referred to as the Big Blue Bump, can extend from the (AGN-frame) optical/UV band to the soft X-ray band and is believed to be thermal emission from the accretion disk [e.g. 44, 45].

The accretion disk is partially covered by a corona of hot - yet still thermal - material. The hot corona Comptonizes some of the emission producing a high-energy tail extending into the hard X-ray regime. Alternative explanations of the origin of the hard X-ray emission include a hot inner flow [e.g. 46, 47], the “lamp-post model” of an X-ray source illuminating the accretion disk from above [e.g. 48, 49], and a structured multilayer corona [50].

In the X-ray spectra of some AGN one detects a broad X-ray emission line at ~ 6.4 keV in the AGN rest frame. The line is believed to be fluorescence Fe K- α emission of iron atoms in the inner accretion disk excited by the hard X-rays from a source above the disk [e.g. 51, 52, 53, 54]. Its shape results from the gravitational redshift incurred by photons climbing out of the black holes gravitational well, and the blue and redshift from the relativistic motion of the disk material. The analysis of the line shape can be used to measure the black hole spin. For the Seyfert galaxy MCG6-30-15, the analysis of the Fe K- α line shape indicates a spin per unit mass of $a > 0.987$ in dimensionless units, close to the theoretical maximum value [55].

Radio interferometric observations at 230 GHz have recently achieved sufficiently good resolutions to resolve the accretion disk of Sgr A*, the 4.5×10^6 M. SMBH at the center of the Milky Way [56]. The radio emission is polarized cyclo-synchrotron emission.

Continuum Emission from the Inner Jet: Under favorable conditions, the accretion leads to the formation of a highly relativistic collimated jet. The make-up of the jet is not well constrained, but is believed to change from magnetic-field-dominated close to the central engine to particle (electron and positron, or ions and electrons) dominated at $> \text{pc}$ distances. Shocks in the jet (e.g. from re-collimation of the jet or plasma instabilities) or reconnection leads to the acceleration of electrons to GeV and TeV energies (Lorentz factors up to a few times 10^6). The electrons emit low-energy synchrotron emission and high-energy inverse-Compton emission. The latter comes from the electrons scattering synchrotron photons (synchrotron self-Compton (SSC) emission) or external photons (external Inverse Compton (EIC) emission), such as BLR photons or photons from upstream or downstream regions of the jet. The continuum emission holds information about the innermost jet regions and can be used for time-dependent studies of particle acceleration processes.

Emission Lines from Clouds: Some AGNs exhibit narrow and/or broad emission lines emitted by rather cold clouds of interstellar material orbiting the black holes at different distances [57]. The broad line region (BLR) clouds have distances on the order of 10 light days from the SMBH; the narrow line region (NLR) clouds orbit the SMBH at distances of a few hundred parsecs. The line centroids can be used to measure the redshifts and thus the distances of AGNs. Observations of the BLR emission and the continuum emission from the accretion disk can be used to estimate the mass of the central black hole based on reverberation mapping [58, 59]. The technique combines the widths of the BLR lines (which constrain the orbital velocities of the emitting clouds) with measured time lags between variations of the continuum flux from the accretion disk and the BLR flux. As the BLR emission stems from reprocessing the continuum flux, the time lag can be used to estimate the distance of the BLR clouds from the central engine. The information about the velocity of the BLR clouds and the distance of the BLR clouds from the SMBH constrain the orbital parameters of the BLR clouds and thus the black hole mass. The technique can be used for AGNs which are so far away that stellar orbits close to the black hole cannot be resolved. Two classical papers

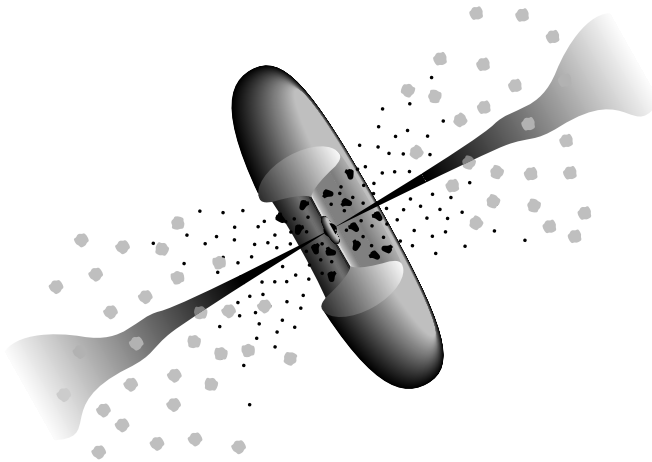


Figure 8: The figure shows a sketch of the central engine of an AGN and highlights several components that can explain most of the observed properties of AGNs (not to scale; example lengths in parentheses). The central black hole (for an $M = 10^8 M_{\odot}$ black hole, the Schwarzschild radius is $R_S = 3 \times 10^{13}$ cm) is surrounded by an accretion disk ($\sim 1 - 30 \times 10^{14}$ cm). The broad emission lines originate in clouds orbiting above the disk (at $\sim 2 - 20 \times 10^{16}$ cm). A thick dusty torus (inner radius $\sim 10^{17}$ cm) or a warped accretion disk obscures the broad-line region (BLR) when the AGN is seen from the side; a hot corona above the accretion disk probably plays a role in producing hard X-rays; narrow lines are produced in clouds much farther from the central source ($10^{18} - 10^{20}$ cm). Radio jets (extending from $\sim 10^{15}$ cm to several times 10^{24} cm) emanate from the region near the black hole in the case of radio loud AGNs. The image does not show the broad and narrow absorption line producing winds. The launching region of the broad absorption line producing winds is uncertain. The narrow absorption line winds are believed to be launched at distances of $\sim 10^{18}$ cm from the central engine at about the same distance from the central engine as the NLR clouds. The graph is reproduced from [43], ©1995 Astronomical Society of the Pacific.

used the line luminosities as estimators of the accretion rate and studied the correlation of line luminosities with the kinematic power of the jet. Rawlings, S., & Saunders [60] estimated the jet power based on the energetics of the radio lobes and correlated the estimated jet power with the [O III] NLR luminosities. The authors found a significant correlation between these two quantities for a sample of radio galaxies. Celotti et al. (1997) [61] found a similar correlation between the BLR luminosities and jet luminosities from very-long-baseline interferometry (VLBI) observations of radio loud AGNs [see also: 62, 63].

Torus and Winds: Some of the differences between observational AGN classes can be explained by the presence of a dusty ~ 1 pc diameter torus which can obscure accretion disk and BLR emission from view and emits reprocessed emission from the central engine in the infrared [64, 65]. At the inner edge of the torus, the AGN continuum emission destroys the dust,

ionizes the atoms and creates the material making up the BLR and X-ray obscuring clouds. The presence of blue-shifted broad (BAL) and narrow absorption lines (NAL) in the optical, UV, and X-ray regime show evidence for fast AGN outflows or winds [66]. While the NAL outflows are believed to be launched at \sim pc distances from the central engine and are largely radiatively driven, the location and the driving mechanism of the fast ($0.2 c$) BAL outflows are still highly uncertain.

At larger viewing angles, the gas torus conceals the BLR and only narrow lines are observed, resulting in Type-2 Seyferts, and narrow line FRI and FRII galaxies. Closer to the line of sight, the torus does not obscure the BLR anymore and the AGNs appear as Type-1 Seyferts, radio quiet quasi-stellar objects (QSOs), and broad line steep spectrum radio quasars (SSRQs) and FSRQs. For viewing angles $< 10^\circ$, the relativistically beamed non-thermal continuum emission from the relativistic jet dominates and the object is a blazar. BL Lac objects are a sub-class of blazars either without detected emission lines or with lines with a rest-frame equivalent width smaller than 5 \AA [67, 68]. Recently, this classification scheme has been criticized on the grounds that it introduces strong selection effects [69, 70].

3.2 Recent Blazar Observations with the Fermi Space Telescope and Imaging Atmospheric Cherenkov Telescopes

In recent years γ -ray astronomy has made spectacular progress. The space-borne Fermi Large Area Telescope (LAT) [71] and ground-based Imaging Atmospheric Cherenkov Telescopes (IACTs) [72] achieve sensitivities of about $10^{-12} \text{ erg cm}^{-2} \text{ s}^{-1}$. The Fermi LAT covers the 100 MeV-300 GeV energy range. With its large field of view ($\sim 2.4 \text{ sr}$) it is well suited to monitor the entire sky on a regular basis. IACTs cover the 50 GeV-30 TeV energy range. With large detection areas on the order of 10^5 m^2 they are well suited to measure short-term ($< 1 \text{ min}$) flux and spectral variability. Between Fermi and the ground-based Cherenkov telescopes, it has become possible to sample the complete inverse Compton emission component of many blazars (Fig. 9).

The γ -ray telescopes detect mostly blazars and make it possible to study the properties of AGN jets on short time scales. In the following we use the abbreviations LSP, ISP and HSP to denote low synchrotron peaked ($\nu_{\text{peak}}^{\text{S}} < 10^{14} \text{ Hz}$), intermediate synchrotron peaked ($10^{14} \text{ Hz} < \nu_{\text{peak}}^{\text{S}} < 10^{15} \text{ Hz}$), and high synchrotron peaked ($\nu_{\text{peak}}^{\text{S}} > 10^{15} \text{ Hz}$) blazars. In the earlier literature, the reader will often find the abbreviations LBL, IBL, and HBL. These names denote the BL Lac subclasses of LSP, ISP, and HSP blazars, respectively.

The large sample of blazars detected by the Fermi-LAT can be used to study the cosmic evolution of blazars as well as the intrinsic properties of blazars. The cosmic evolution of blazars depends on the cosmic evolution of SMBHs, the accretion history of these SMBHs, and the history of the radiative efficiency of the accreting SMBHs. The recently published second Fermi LAT AGN catalog [75] lists 1017 sources with an AGN association, and a “clean sample” of 886 sources with unambiguous AGN counterparts. The latter sample includes 395 BL Lacs, 310 FSRQs, 157 candidate blazars of unknown type, eight misaligned AGNs, four narrow-line Seyfert 1 galaxies,

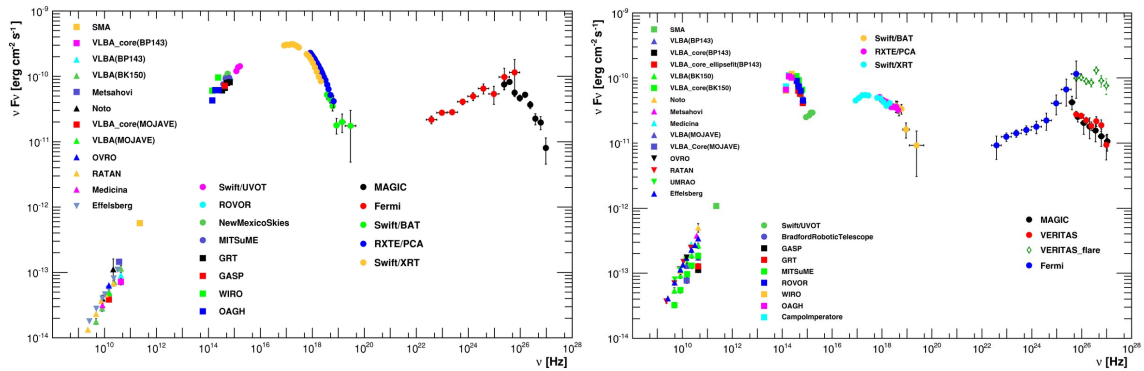


Figure 9: Broadband spectral energy distribution of the HSP blazars Mrk 421 (left panel, data taken between January 19, 2009 and June 1, 2009) and Mrk 501 (right panel, data taken between March 15, 2009 and August 1, 2009). The images are reproduced from Refs. [73] (left panel) and [74] (right panel), ©2011 American Astronomical Society.

ten AGNs of other types, and two starburst galaxies. The redshift distribution (dN/dz) of detected BL Lacs peaks at $z \approx 0.2$ and extends to $z = 1.5$; the distribution of FSRQs peaks at $z \approx 1.1$ and extends to $z = 3.2$.

Ajello et al. (2012) use a complete sample of FSRQs detected during Fermi’s first year of operation to study the luminosity function (LF) and its cosmic evolution [76]. The FSRQ number density grows up to luminosity dependent redshifts of between 0.5 and 2.0 and declines thereafter. The sources show an “inverted evolution” with lower power sources peaking at lower redshifts (later times) than their higher-power counterparts (Fig. 10, left panel). The authors study the rest-frame spectral energy distribution (SED, energy flux per logarithmic energy interval, $E^2 dN/dE$) of the sources and find that the peak of average SEDs determined for different luminosity bins is independent of the AGN luminosity (Fig. 10, right panel). The earlier detection of a luminosity-hardness correlation (sometimes referred to as the “blazar sequence”) [77, 78] may have resulted from selection effects. Combining the inferred SED shapes with the LF, the authors predict that FSRQs contribute $\sim 10\%$ to the isotropic Fermi γ -ray background. Assuming that the jet Bulk Lorentz factors Γ_j follow a power law distribution $dN/d\Gamma_j \propto \Gamma_j^k$ over the range from 5 to 40 and that the γ -rays originate as SSC emission, the authors can derive the distribution of intrinsic jet luminosities \mathcal{L} from the distribution of apparent luminosities L (for SSC emission, $L \propto \delta_j^p \mathcal{L}$ with $p = 4$). The analysis implies a power law index k of -2.0 ± 0.7 , a mean Lorentz factor of the Fermi-detected FSRQs of ≈ 12 , that most sources are seen from within 5° of the jet axis, and that the detected γ -ray loud FSRQs represent 0.1% of the unbeamed parent population. The distribution of Γ_j is in good agreement with those inferred from radio observations on pc-scales [20]. The finding may imply that both, the radio and the γ -ray emission comes from \sim pc-distances from the central engines, or, that the jet Lorentz factors are the same at the scales probed by the

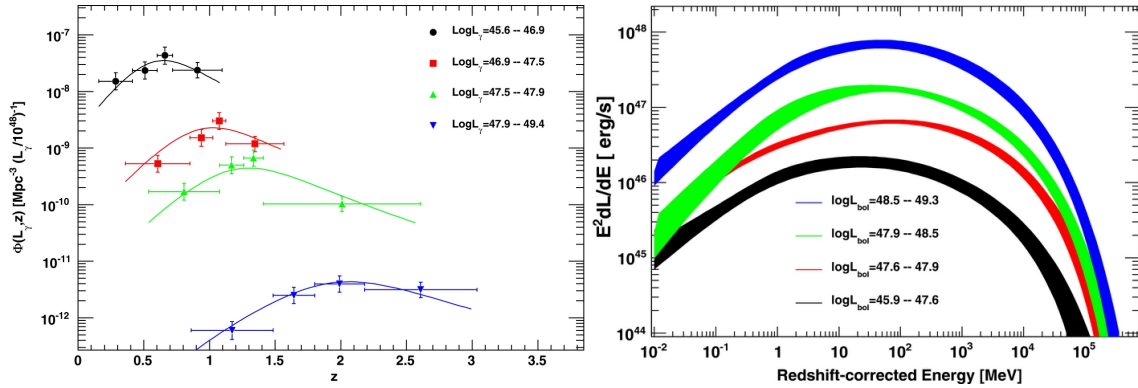


Figure 10: Left panel: space density of Fermi-LAT detected FSRQs for different luminosity classes indicated an “inverted hierarchy” with higher (lower) luminosity objects peaking at higher (lower) redshifts. Right panel: average rest-frame spectral energy distributions for four FSRQ luminosity classes. The bands show the 1σ confidence level regions [from 76]. The data do not indicate a correlation of the energy at which the spectral energy distribution peaks and the γ -ray luminosity. The images are reproduced from Ref. [76], ©2012 American Astronomical Society.

radio and γ -ray observations.

Ghisellini et al. (2012) study the correlation between the BLR luminosity L_{BLR} and the γ -ray luminosity L_γ , both measured in units of the Eddington accretion rate, and find a correlation albeit with a large scatter [29]. The result reinforces the earlier finding that accretion rate (and thus L_{BLR} and jet power (proportional to L_γ) are correlated, but shows that it is even valid when both are normalized to the mass of the black hole.

Giommi et al. (2012) report on a Monte Carlo study that shows that selection effects can strongly affect the outcomes of BL Lac and FSRQ studies [70]. Their work indicates that selection effects alone can produce an apparent correlation between the peak energy of the synchrotron SED and the luminosity of the sources. The analysis suggests that powerful BL Lac-type objects may exist, but cannot be identified as such owing to the relative weakness of the lines. In their model, all sources are qualitatively the same, but are identified as different sources owing to the relative strength of several basic emission components, i.e. the Doppler boosted radiation from the jet, the emission from the accretion disk, the BLR, and the light from the host galaxy. The authors suggest that – using the standard definitions – BL Lacs and FSRQs may not be the beamed versions of FRI and FRII, respectively. Ghisellini et al. (2011) offer a definition of BL Lacs and FSRQs based on the broad line region luminosity in units of the Eddington luminosity ($L_{\text{BLR}}/L_{\text{Edd}}$ below and above 5×10^{-4} , respectively) [69], which might result in a cleaner identification of the beamed versions of FRI and FRII galaxies.

IACTs and the Fermi LAT have been used for extensive multiwavelength campaigns. For HSP blazars, the broadband SEDs [e.g. 79, 80] and fast flux variability [81, 82, 83, 84] imply

very high relativistic Doppler factors δ_j (Equation (3)) on the order of 50. The broadband SEDs can largely be fit with one-zone SSC models [e.g. 85, 86] with notable exceptions [e.g. 87, 88]. Snapshot and time-dependent modeling indicates particle dominated emission zones with electron and positron energy densities $u_{e+/-}$ exceeding the magnetic field energy density $u_B = B^2/8\pi$ by typical factors of ~ 100 [79, 85]. Models with additional target photon fields (and with additional degrees of freedom) make it possible to fit the data closer to equipartition ($u_{e+/-} \sim u_B$) [89, 90].

LSP and ISP blazars seem to require EIC models. Abdo et al. (2010) discuss the broadband SEDs of 48 γ -ray bright Fermi blazars [91]. The authors find that one-zone SSC models cannot fit the SEDs of most LSP and ISP (low frequency peaked BL Lac objects and FSRQs) sources [see also: 92].

Broadband observations promise to give insights into the mechanisms responsible for the observed flares. There is good evidence for a correlation of the radio and > 100 MeV γ -ray luminosities of statistical samples of blazars [92, 94, 95, 96], and to some degree of the X-ray and VHE (Very High Energy, >100 GeV) γ -ray fluxes of HSP blazars (e.g. Fig. 11 and [93, 97]). Marscher et al. (2008) [98] and Abdo et al. 2010 [99] report the detections of correlated polarization swings and γ -ray flares. Unfortunately, the interpretation of some of the data is rather ambiguous as the sources exhibit a wide range of different behaviors; as a consequence, the statistical significance of the observed features is often rather limited. Unambiguous conclusions would require the observation of a statistical sample of sources with dense sampling in the temporal and waveband domains over many years.

The continuum emission from blazars is most commonly explained in the framework of electron and possibly positron acceleration in internal or external collision-less shocks. The accelerated leptons radiate synchrotron radio to X-ray and inverse-Compton X-ray to gamma-ray emission. Unfortunately, attempts to verify that Fermi-type acceleration energizes the leptons based on observations of predominantly clockwise or counterclockwise loops in the flux vs. spectral index plane [e.g. 100] failed due to the rather chaotic behavior of the observed sources [e.g. 101, 102].

Some authors consider hadronic models in an attempt to explain the γ -ray emission from blazars, but such models require the acceleration of protons to $> 10^{18}$ eV energies and magnetic fields typically on the order of ~ 50 G with very high energy densities to accelerate and confine the protons [103, 104, 105, 106, 107].

3.3 Models of the Accretion Flow and Jet Formation

A satisfactory model of the central engines of AGNs should explain (i) how matter and magnetic fields are transported towards the accretion disks of the SMBHs; (ii) which types of accretion disks occur in nature and how they work; (iii) which physical mechanisms are responsible for accretion disk state transitions and flares; (iv) how the individual emission components are produced, (v) how jets form, transform, accelerate and/or decelerate at different distances from the SMBHs; (vi) how AGNs interact with their environment. The question of how matter and magnetic fields move towards the central engine (the feeding problem) will not have a simple answer as it will depend on the cosmic epoch and the type and evolutionary state of the host (a single galaxy or a galaxy

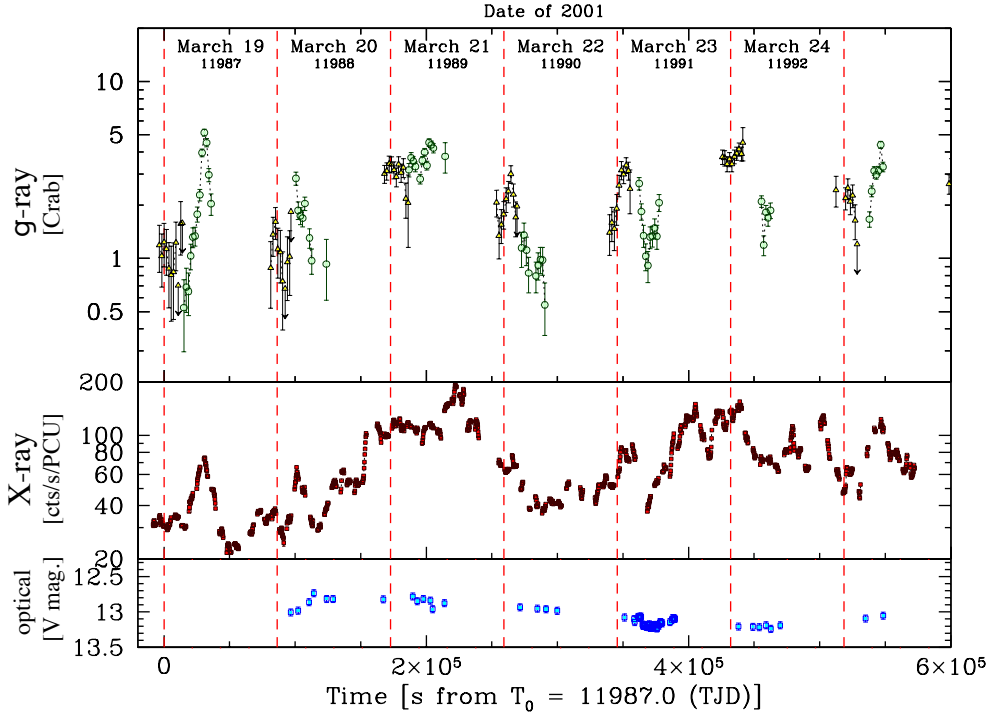


Figure 11: Results from 2001 Rossi X-ray Timing Explorer (*RXTE*) 2-4 keV X-ray and Whipple (full symbols) and HEGRA (open symbols) γ -ray observations of Mrk 421 in the year 2001 [from 93]. IACTs achieve excellent sensitivities on short time scales owing to their large collection areas. Careful study of the light curves shows that the X-ray and TeV γ -ray fluxes are correlated for some flares but not for all. Reproduction of the figure with kind permission of the authors.

inside a galaxy cluster). The main challenge is to explain how the matter can shed all but a tiny fraction of its initial angular momentum while it goes through different phases and moves from \sim kpc distances to the accretion disk [e.g. 40, 108]. One of the open questions concerns the feeding of magnetic fields with a preferred polarity into the accretion flow, as such magnetic fields can suppress plasma instabilities in the disk, and can explain the presence of a strong single polarity magnetic field in the surrounding of the black hole, i.e. in the plunging region between the event horizon and the innermost circular stable orbit (ISCO). Such magnetic fields are required in some models of accretion and jet formation.

Accretion disks transform gravitational energy of matter into electromagnetic and mechanical energy. Shakura & Sunyaev (1973) introduced a model for a geometrically thin (with a thickness H at radius r such that $H(r)/r \ll 1$), optically thick accretion disk [109]. Assuming that the disk matter orbits the black hole on circular geodesics, that there is no torque at the ISCO, that the disk radiates away all the dissipated energy, and that no heat is transported in radial direction, the radial

structure of the disk is entirely determined by mass, energy, and angular momentum conservation [109, 110]. Using a prescription for the viscosity of the disk, the horizontal disk structure can be inferred. Although it was suspected that magnetic turbulence caused by the differential rotation of the accretion disk material was responsible for the viscosity, it was only in 1991 that Balbus & Hawley identified the magneto-rotational instability (MRI) as the driving instability based on numerical simulations [111].

A number of authors discuss alternative accretion flows. Ichimaru (1977) describes a two-state model to explain two qualitatively different emission states of the X-ray binary Cygnus X-1 [46]. Whereas the high-soft state corresponds to the geometrically thin, optically thick radiatively efficient accretion disk of Shakura & Sunyaev, the low-hard state corresponds to a geometrically thick, optically thin radiatively inefficient accretion flow (RIAF). In the latter case, a thermal instability of the disk plasma develops when dissipative heating exceeds the radiative cooling causing the disk to puff up. Narayan et al. (1994) discusses a self-similar geometrically thick RIAF flow, the advection dominated accretion flows (ADAFs), in which the gas orbits the black hole with a velocity well below that of Keplerian orbits [112]. The authors remark that such flows can form for low accretion rates when the flow is optically thin, or for very high accretion rates when the flow is optically thick and the cooling time of the plasma is much longer than the accretion rate. Variations of ADAFs include convection-dominated accretion flows (CDAFs) [113, 114], and advection-dominated inflow-outflow solutions (ADIOSs) [115, 116].

The jet is probably launched by the combined effect of thermal pressure, centrifugal forces, and the Blandford-Znajek process. The latter involves the conversion of the rotational energy of a black hole spinning in the magnetic field anchored in the accretion disk into electromagnetic energy [117]. In the presence of a favorably shaped outflow channel (formed by a geometrically thick accretion disk or by a less collimated wind), the flow can accelerate owing to magnetic pressure gradients. Energy conservation dictates that the terminal Lorentz factor of the jet obeys $\Gamma_j^\infty < \sigma_0$ with σ_0 being the magnetization (ratio of electromagnetic to particle energy densities) at the base of the jet, so that $\sigma \gg 1$ is required to explain $\Gamma_j^\infty \gg 1$.

We would like to know which accretion flows occur in nature, which flow properties lead to the observed phenomenology, and how the observed jets form. Attempts in this direction include the identification of the radio quietness and loudness (the absence or presence of a jet) with geometrically thin and geometrically thick accretion flows, respectively. Some authors explain the difference between BL Lacs and FSRQs by invoking radiatively inefficient (with weak BLR emission) accretion flows for the former and radiatively efficient (strong BLR emission) accretion flows for the latter sources. Unfortunately, none of these associations is firm at the time of writing.

Recently it has become possible to employ 2D and 3D general relativistic magnetohydrodynamic (GRMHD) simulations with sufficient resolution to test some of the assumptions underlying the analytical and semi-analytical models. Most simulations neglect radiative transfer of heat owing to computational limitations. Such simulations have been used, for example, to test the assumption of zero torque at the ISCO (and zero energy dissipation of the disk plasma within the ISCO). The results indicate that the zero-torque approximation introduces rather small errors, i.e. it underestimates the emitted luminosity by $\sim 5\%$ [118, 119]. McKinney et al. (2012) studied rather thick

($H/r \sim 0.3$) accretion flows with large-scale dipole and quadrupole magnetic fields and obtained two interesting results [40]: (i) the structure of the accreted magnetic field is decisive for the formation of a collimated relativistic outflow; an accretion disk with a dipole magnetic field geometry does produce a jet, but disks fed by plasma without an ordered magnetic field or with higher moment magnetic field geometries do not [see also: 120, 121]; (ii) somewhat unexpectedly, the jets are stable even though the toroidal component of the magnetic field that accelerates the jets could disrupt the flow owing to helical kink and screw modes. Several effects – including gradual shear, stabilizing sheaths, or sideways expansion – may be responsible for stabilizing the outflow.

As ordered magnetic fields are needed for the production of jets, McKinney et al. (2012) employ 3D GRMHD simulations to study a geometrically thick flow supplied with strongly magnetized plasma [40]. They find that for rapidly spinning black holes toroidal magnetic fields can lead to large patches of single-polarity poloidal magnetic fields threading the black hole enabling the transformation of rotational energy of the black hole into Poynting flux energy. Strong poloidal magnetic fields build up in the inner region of the disk and compress it into a geometrically thin accretion flow in which the strong poloidal magnetic field suppresses the MRI. As mentioned above, further studies are needed to understand which accretion flows are actually realized in nature.

4 The Cosmic History of Black Hole Accretion

Most current black hole formation models tell us that the first black hole seeds emerged at $z \gtrsim 15$. While the exact mechanism is not known, there are several prevailing theories (see the comprehensive reviews by M. Rees [122] and M. Volonteri [123] for more details). One possibility is that the first black holes were the remnants of the first generation of stars (Population III stars) that resulted from the gravitational collapse of primordial ultra-low metallicity gas. These black holes formed at $z \sim 20$ and have typical masses ~ 100 - $1,000 M_{\odot}$. This scenario has problems explaining the very high masses, of $\sim 10^9 M_{\odot}$, estimated for supermassive black holes in $z > 6$ optically-selected quasars [124, 125]. Alternatively, the first black holes could have formed directly as the result of gas-dynamical processes. It is possible for metal-free gas clouds with $T_{vir} \gtrsim 10^4 \text{K}$ and suppressed H_2 formation to collapse very efficiently [126], possibly forming massive black hole seeds with $M \sim 10^4$ - $10^5 M_{\odot}$ as early as $z \sim 10$ - 15 . If instead the UV background is not enough to suppress the formation of H_2 , the gas will fragment and form “normal” stars in a very compact star cluster. In that case, star collisions can lead to the formation of a very massive star, that will then collapse and form a massive black hole seed with mass $\sim 10^2$ - $10^4 M_{\odot}$ [127].

Given the current typical masses of $10^{6-9} M_{\odot}$, most black hole growth happens in the AGN phase [128, 129]. With typical bolometric luminosities $\sim 10^{45-48} \text{erg s}^{-1}$, AGN are amongst the most luminous emitters in the Universe, particularly at high energies and radio wavelengths. These luminosities are a significant fraction of the Eddington luminosity — the maximum luminosity for spherical accretion beyond which radiation pressure prevents further growth — for a $10^{8-9} M_{\odot}$ central black hole. A significant fraction of the total black hole growth, $\sim 60\%$ [130], happens in the most luminous AGN (quasars) which are likely triggered by the major merger of two massive

galaxies, as it is discussed in Sect. 5. In the quasar phase, which lasts $\sim 10^8$ years, the central supermassive black hole can gain up to $\sim 10^7$ - $10^8 M_\odot$, so even the most massive galaxies will have only a few of these events over their lifetime. Further black hole growth, mostly in low-luminosity (low Eddington rate) AGN, is likely due to stochastic accretion of cold gas, mostly in spiral galaxies [131].

According to the AGN unification paradigm [43, 132], a large fraction of these sources, $\sim 75\%$ locally, are heavily obscured by optically and geometrically thick axisymmetric material, which explains many of the observed differences among different types of active galaxies. In addition, luminosity [133] and cosmic epoch [134] play a significant role. One constraint on the fraction of obscured AGN and its evolution comes from the spectral shape of the extragalactic X-ray “background” (XRB). Thanks to deep X-ray observations at $E \lesssim 10$ keV performed by Chandra and *XMM-Newton*, a very large fraction of the X-ray background, $\sim 80\%$, has been resolved into point sources [135], the vast majority of them AGN [136]. Several studies, the first of them ~ 20 years ago [137], have used a combination of obscured and unobscured AGN to explain the spectral shape and normalization of the X-ray background with overall good results. The latest AGN population synthesis models [138, 139] assume an average ratio of obscured to unobscured AGN of $\sim 3:1$ locally, increasing towards lower luminosities and higher redshifts, as well as a fraction of Compton-thick sources (CT; $N_H > 10^{24} \text{cm}^{-2}$) of ~ 5 - 10% , consistent with the value observed at higher energies, $E=10$ - 100 keV, of $\sim 5\%$ by *INTEGRAL* in the local Universe [138, 140], lower by factors of ~ 3 than expectations of previous population synthesis models [141, 142].

Direct black hole mass measurements, either through stellar or gas dynamics, are available only for a few nearby galaxies. However, thanks to the tight correlation between the mass of the supermassive black hole and other properties (such as velocity dispersion), it has been possible to estimate the black hole mass function at $z \simeq 0$ [143, 144, 145, 146]. This is commonly done starting from the observed galaxy luminosity or velocity function and assuming either a constant black hole to stellar mass ratio [143] or the M - σ relation [145]. Both the overall shape of the black hole mass function and the integrated black hole mass density, which can only be computed at $z \simeq 0$, can be used to infer properties of the AGN population. This was first used in the so-called “Soltan’s argument” [129], which says that the intrinsic bolometric AGN luminosity, L , is directly linked to the amount of mass accreted by the black hole, \dot{M}_{acc} :

$$L = \varepsilon \dot{M}_{acc} c^2,$$

where ε is the accretion efficiency and c is the speed of light. A typical value assumed for the efficiency is $\sim 10\%$ [129, 145].

Recent comparisons of the black hole mass function to the distribution inferred from the observed AGN luminosity indicate that the average efficiency is 8% , the Eddington ratio is $\sim 50\%$, and the average lifetime of the visible AGN phase is $\sim 10^8$ years [145, 146]. By studying the black hole mass distribution at the high mass end, $M > 10^9 M_\odot$, Natarajan & Treister [147] found that the observed number of ultra-massive black holes is significantly lower than the number density inferred from the AGN hard X-ray luminosity function. They concluded that this is evidence for

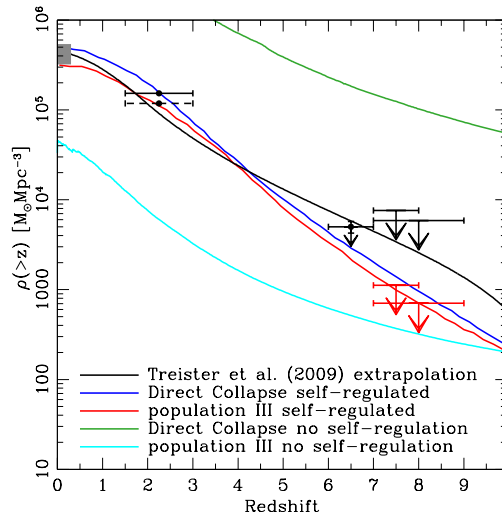


Figure 12: Total accreted mass by supermassive black holes per cubic megaparsec as a function of redshift. The *gray rectangle* shows the range of values allowed by observations of $z \simeq 0$ galaxies [148]. The data points at $z \sim 2$ correspond to the values obtained from Chandra observations of X-ray detected AGN and luminous infrared galaxies [130], while the upper limits at $z > 6$ show the results described in [149] (*red* and *black* data points from the observed-frame soft and hard X-ray band observations respectively). The *black* solid line shows the evolution of the total accreted mass per proper volume element inferred from the extrapolation of AGN luminosity functions measured at lower redshifts [138]. We over-plot the predictions of black hole and galaxy evolution models [123] for non-regulated growth of Population-III star remnants (*cyan line*) and direct-collapse seeds (*green*). The *red* and *blue* lines show the predicted BH mass density if self-regulation is incorporated.

an upper limit to the black hole mass, which can be explained by the presence of a self-regulation mechanism.

The observed black hole mass density at $z \simeq 0$ obtained by integrating the black hole mass function, ranges from 2.9×10^5 [144] to $4.6^{+1.9}_{-1.4} \times 10^5 \text{ M}_\odot \text{ Mpc}^{-3}$ [145]; more recently, Shankar et al. (2009) found $3.2\text{-}5.4 \times 10^5 \text{ M}_\odot \text{ Mpc}^{-3}$ [148]. For comparison, integrating the AGN hard X-ray LF, including the number of Compton-thick AGN constrained by *INTEGRAL* and Swift/BAT observations, Treister et al. obtained a value of $4.5 \times 10^5 \text{ M}_\odot \text{ Mpc}^{-3}$, perfectly consistent with the observed value, indicating that at least locally, X-ray detected AGN can account for most or all of the black hole growth [138]. A comparison between the observed black hole mass density at $z \simeq 0$ and the value derived from integrating the AGN luminosity function is shown in Figure 12.

At higher redshifts, the black hole mass density at $z \sim 1\text{-}3$ can be derived from the Chandra observations of X-ray detected AGN and luminous infrared galaxies at $z \sim 2$ [130]. Upper limits

to the observed black hole mass density at $z > 7$ were obtained from X-ray stacking at the position of high-redshift galaxy candidates in the Chandra Deep Field South by [149]. Although a strong detection at $z \sim 6$ was reported [149], it was recently questioned by other authors [150, 151]. In the following, we treat the detection as an upper limit. The measurements can be compared to the expectations derived from black hole growth models. In particular, we use as a comparison the results in [152], [153] and [154]. Two “seed” formation models are considered : those deriving from population-III star remnants (Pop III), and from direct collapse models (D.C.). In this scheme, the central black holes accumulate mass via accretion episodes that are triggered by galaxy mergers. Accretion proceeds in one of two modes: self-regulated or un-regulated. For each black hole in these models we know its mass at the time when the merger starts (M_{in}), and we set the final mass through the self-regulated or un-regulated prescription. These two models differ by the amount of mass a SMBH accretes during a given accretion phase. As it can be seen in Fig. 12, models that do not incorporate the effects of self-regulation in black hole growth are grossly inconsistent with the available observational data.

While a clear picture of the history of black hole growth is emerging, significant uncertainties still remain. In particular, while the spectral shape and intensity of the extragalactic X-ray background have been used to constrain the AGN population, the number of heavily obscured accreting supermassive black holes beyond $z \sim 1$ is not properly bounded. Infrared and deep X-ray selection methods have been useful in that sense, but have not provided a final answer, due to confusion with star-forming galaxies in the infrared and the effects of obscuration in X-rays. At higher redshifts, the situation is even more unclear, and only a few, very rare, high luminosity quasars are known. Unless high-redshift AGN luminosity functions are pathological, these extreme sources do not represent the typical growing black holes in the early Universe. As a consequence, and in spite of recent advances [149, 155], the formation mechanism for the first black holes in the Universe is still unknown.

5 What Triggers Black Hole Growth?

While it is clear now that most galaxies contain a supermassive black hole in their center, only a small fraction of these black holes are AGNs. This indicates that black hole growth is most likely episodic, with each luminous event lasting $\sim 10^7$ - 10^8 years [156]. An obvious question is: What triggers these black hole growth episodes?

Major galaxy mergers provide a good explanation, since, as simulations show, they are very efficient in driving gas to the galaxy center [157], where it can be used as fuel for both intense circumnuclear star formation and black hole growth. Indeed, a clear link between quasar activity and galaxy mergers has been seen in intensely star-forming galaxies like ultra-luminous infrared galaxies (ULIRGs) and in some luminous quasars [e.g., 158]. In contrast, many AGN are clearly not in mergers or especially rich environments [159]. Instead, minor interactions [160], instabilities driven by galaxy bars [161] and other internal galaxy processes might be responsible for these lower activity levels. Understanding the role of mergers is further complicated by the difficulty of

detecting merger signatures at high redshifts.

In order to reconcile these potentially contradictory observations, it has been suggested that the AGN triggering mechanism is a function of luminosity and/or redshift [162, and others]. More recently, Hopkins & Hernquist [163] used five indirect tests to conclude that the triggering mechanism is strongly luminosity-dependent and more weakly redshift-dependent, so that only the most luminous sources, which are preferentially found at $z > 2$, are triggered by major mergers [163]. Thanks to results from large AGN surveys, which now include heavily-obscured IR-selected sources, and recent deep high-resolution observations carried out with the *Hubble* WFC3 detector, it is now possible to obtain reliable morphological information even for high- z , low luminosity sources.

To measure the fraction of AGN hosted by a galaxy undergoing a major merger as a function of luminosity and redshift, Treister et al. (2012) compiled information from AGN samples selected from X-ray, infrared and spectroscopic surveys [164]. They studied data from 10 independent surveys, which include 874 AGN, spanning a wide range in luminosities, $3 \times 10^{42} < L_{bol}(\text{erg s}^{-1}) < 5 \times 10^{46}$, and redshift, $0 < z < 3$. The goal of their work is to determine the physical mechanism(s) that provoked the AGN activity identified in these surveys. Only visual morphological classifications have been used, as they are the reliable option to determine if a galaxy is experiencing a major merger [165]. The fraction of AGN linked to galaxy mergers in these samples has been computed by dividing the number of AGN in which the host galaxy has been classified as an ongoing merger or as having major disturbances by the total number of AGN. Figure 13 shows the fraction of AGN showing mergers as a function of bolometric luminosity, which increases rapidly, from $\sim 4\%$ at $10^{43} \text{ erg s}^{-1}$ to $\sim 90\%$ at $10^{46} \text{ erg s}^{-1}$.

The spectral shape and intensity of the X-ray background can tell us about the average properties of the AGN population. Using the models of [138] with the AGN luminosity function of [166] and the luminosity dependence of the fraction of AGN triggered by major mergers, we can estimate their contribution to the background radiation in X-rays. In Figure 14 we show separately the contributions to the X-ray background from AGN triggered by secular processes and major mergers, which contribute nearly equally to the X-ray background. This is because most of the X-ray background comes from $z < 1$ sources [e.g., 138], where AGN activity due to secular processes is relatively more important. This is particularly true at $E > 10 \text{ keV}$, where AGN emission is roughly unaffected by obscuration. Because of the luminosity dependence of the fraction of obscured AGN [e.g., 167], AGN triggered by secular processes are relatively more obscured than those attributed to major galaxy mergers, which explains the different spectral shapes in Figure 14 and the fact that AGN triggered by mergers are more important at $E < 5 \text{ keV}$. We note that a population of high-luminosity heavily-obscured quasars likely associated with major mergers have been reported by [130] and others. These sources are mostly found at $z \sim 2$ and show evidence of very high, Compton thick, levels of obscuration. Hence, these sources do not contribute significantly to the X-ray background radiation at any energy.

In Figure 15 we show, as a function of redshift, the amount of black hole growth and number of AGN triggered by major galaxy mergers relative to those associated with secular processes. As can be seen and was previously reported [e.g., 130], black hole growth occurs mostly in accretion

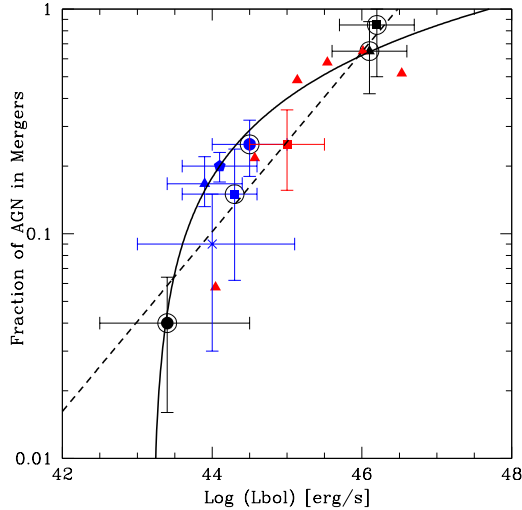


Figure 13: Fraction of AGN showing mergers as a function of the AGN bolometric luminosity. Colors indicate AGN selection method (*red*: infrared, *blue*: X-rays, *black*: optical) (from [164]). Encircled symbols show samples at $z < 1$. *Solid line* shows a fit to the data assuming a linear dependence of the fraction on $\log(L_{bol})$, while the *dashed line* assumes a power-law dependence.

episodes triggered by major galaxy mergers, although secular processes are still important. This is particularly true at $z \gtrsim 2$, where there is $\sim 60\%$ more black hole growth in merger-triggered AGN than in those growing via secular processes. At lower redshifts, there are relatively fewer galaxy mergers and so secular processes become slightly more important. Furthermore, at lower redshifts dry mergers become more common than gas-rich major mergers [168]. Since the availability of gas is a critical factor in determining the black hole accretion rate, this further explains why major mergers are relatively more important at high redshifts. It is interesting to note that the diminishing role of mergers coincides with the decline in the space density of black hole growth and with the observed decline in the cosmic star formation rate [169], i.e., cosmic downsizing. Integrated over the whole cosmic history, to $z=0$, 56% of the total black hole growth can be attributed to major galaxy mergers.

In terms of numbers, the population is strongly dominated by secularly-triggered AGN. Indeed, as can be seen in Figure 15, $\sim 90\%$ of AGN at all redshifts are associated with secular processes. This explains the conclusions of previous studies, mostly based on X-ray surveys [e.g. 170, 171, 172] of moderate luminosity AGN, which found that normal disk-dominated galaxies constitute the majority of the AGN host galaxies. We conclude that while most AGN are triggered by secular processes, most of the black hole growth, particularly at high redshifts, can be attributed to intense accretion episodes linked to major galaxy mergers.

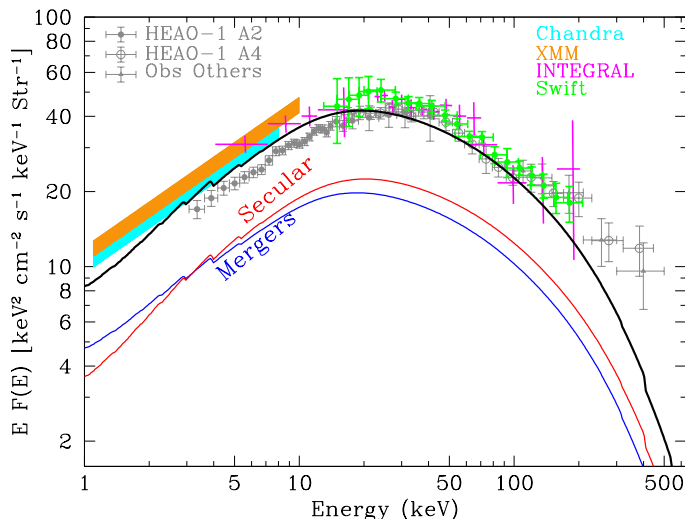


Figure 14: Spectral energy distribution of the extragalactic X-ray background, as a function of observed-frame energy. Observational data points are summarized in [138]. Merger-triggered AGN (*blue line*) contribute roughly equal amounts of light as black hole growth (*red line*). Most of the X-ray background emission comes from $z < 1$ [138], hence the relative importance of secularly-triggered AGN. The extragalactic background light from higher redshift AGN peaks in the optical/UV and is dominated by luminous, merger-triggered AGN. The spectral shapes of the merger and secular contributions are slightly different since the fraction of obscured sources is a function of luminosity.

6 Outlook

The recent progress in our understanding has come from a fleet of telescopes and from the possibility to test accretion disk, jet, and particle acceleration models with numerical codes. On the observational side, we expect further progress from several observatories; for example:

mm and Sub-mm Radio Emission: the Atacama Large Millimeter Array (ALMA) will revolutionize our understanding of galaxy evolution. Sources of mm and sub-mm emission traced by ALMA include thermal emission of the warm/cold dust, which traces star formation, synchrotron radiation associated with relativistic particles and free-free radiation from HII regions. In particular, CO rotational transition lines have been used to trace the spatial distribution, kinematics, temperature and mass of the molecular gas [173]. The sensitivity of ALMA will allow for the detection of luminous IR galaxies ($L_{\text{IR}} > 10^{11} L_{\odot}$), which have been found to often host a heavily-obscured AGN [174], up to $z \sim 10$. Furthermore, with ALMA it will be possible to study separately the molecular dust surrounding the central black hole and those in star forming regions in the host galaxy. Due to their limited sensitivity and

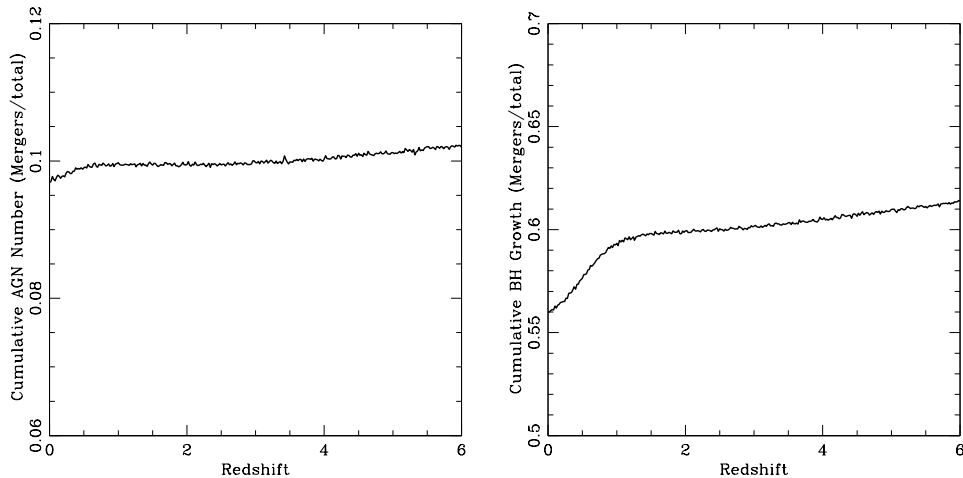


Figure 15: *Left panel:* Cumulative number of merger-triggered AGN relative to the total number of AGN as a function of redshift (from: [164]). While secular-triggered AGN vastly outnumber those triggered by major mergers, by about a factor of ~ 10 , the latter are on average significantly more luminous, thus explaining why they constitute $\sim 60\%$ of black hole accretion. *Right panel:* Cumulative fraction of black hole accreted mass in AGN triggered by mergers as a function of redshift, assuming a constant efficiency for converting mass to light. Black hole accretion is dominated by merger-triggered AGN at all redshifts but especially at $z > 1$. At $z \sim 1$, the much lower gas and merger fractions lead to a dominance of secular processes in AGN accretion.

angular resolution, currently-available mm/sub-mm telescopes are not ideal to study star-forming regions even in nearby galaxies. This will dramatically change thanks to ALMA, which will have orders of magnitude better sensitivity and HST-like angular resolution. The first call for ALMA observations was released on March 31, 2011, for observations starting on September 30, 2011. It is expected that the complete array will be in full operation in 2013. The superb spatial resolution and sensitivity of ALMA will allow the identification of the optical/near-IR counterpart of the mm-submm sources. Furthermore, ALMA will directly provide the redshift of the mm-submm sources through the detection of CO rotational transition lines, up to very high redshifts. Combining these new data with existing multi-wavelength information will finally allow us to complete the census of supermassive black hole growth since the epoch of cosmic re-ionization.

Using (sub)mm observatories around the world for very long baseline interferometry, it should be possible to achieve angular resolutions on the order of $20 \mu\text{as}$ [175]. Such angular resolutions, corresponding to a few gravitational radii of the SMBHs in the Milky Way and in the nearby radio galaxy M87, may allow us to observe the shadow of these two SMBHs.

The measurements would provide direct evidence for the presence of an event horizon; furthermore, they would allow us to measure the Sgr A* and M87 SMBH spins, and to perform rough tests of GR in the strong gravity regime.

Hard X-rays: launched in June 2012, NuSTAR is the first focusing hard X-ray (5-80 keV) X-ray mission, reaching flux limits ~ 100 times fainter than *INTEGRAL* or *Swift*/BAT observations and comparable to Chandra and *XMM-Newton* at lower energies. During the first two years of operations, NuSTAR observes, as part of the guaranteed time program, two extragalactic fields: the ECDF-S and the central 1 deg^2 part of COSMOS, for a total of 3.1 Msec each. These deep high-energy observations will enable us to obtain a nearly complete AGN survey, including heavily-obscured Compton-thick sources, up to $z \sim 1.5$ [176]. A similar mission, ASTRO-H [177], will be launched by Japan in 2014. Both missions will provide angular resolutions $\lesssim 1'$, which in combination with observations at longer wavelengths will allow for the detection and identification of most growing supermassive black holes at $z \sim 1$. Balloon-borne hard X-ray polarimeters [178, 179] might succeed to measure the polarization of the hard X-ray emission from bright AGN jets. The observations could shed light on the magnetic field structure in HSP blazars and could distinguish between an SSC and EIC origin of the inverse-Compton emission of LSP and ISP sources [180].

γ -Rays: the VERITAS array of IACTs has been upgraded in summer 2012 to observe the northern $> 100 \text{ GeV}$ γ -ray sky with a 30% improved sensitivity. The H.E.S.S. collaboration announced first light observations with a large 600 m^2 Cherenkov telescope in July 2012 which will enable observations down to energies of 50 GeV. Together with the Fermi LAT and MAGIC, these experiments will scrutinize the γ -ray sky with unprecedented sensitivity. Long-term monitoring programs enabled by Fermi LAT's quasi-continuous sky coverage and multiwavelength campaigns with all the γ -ray telescopes will clarify the existence or non-existence broadband flux and spectral correlations giving us more detailed information about the properties of AGN jets at their bases.

Other experiments, currently in the proposal stage, could revolutionize our understanding of AGNs, including a *LISA*-type space-based gravitational wave mission (tests of GR, insights into the formation and growth of SMBHs from SMBH spin measurements, [e.g. 181]), an *IXO*-type high-throughput soft X-ray observatory (measurement of the spins of a sample of SMBHs through Fe K- α observations) [182], a *GEMS*-type high-sensitivity X-ray polarimeter (geometry of accretion disk coronae and magnetic field structure in jets) [183], and the next-generation Cherenkov Telescope Array (time resolved observations of blazars and mapping of the γ -ray emission from radio galaxies) [184].

Acknowledgements

HK acknowledges support from NASA (grant NNX10AJ56G), and the Office of High Energy Physics of the US Department of Energy. ET received partial support from Center of Excellence in

Astrophysics and Associated Technologies (PFB 06) and from FONDECYT grant 1120061. The authors thank A. McCollum for help with the references. Special thanks go to Dan Harris and Anca Parvulescu and to the editors Bing Zhang and Peter Meszaros for carefully reading the manuscript and providing excellent comments.

References

- [1] Magorrian, J., et al., “The Demography of Massive Dark Objects in Galaxy Centers”, *AJ*, vol. 115, pp. 2285–2305, June 1998.
- [2] Gültekin, K., et al., “The M - σ and M - L Relations in Galactic Bulges, and Determinations of Their Intrinsic Scatter”, *ApJ*, vol. 698, pp. 198–221, June 2009.
- [3] Psaltis, D. 2008, ”Probes and Tests of Strong-Field Gravity with Observations in the Electromagnetic Spectrum”, *Living Rev. Relativity* 11, (2008), 9. URL (cited on 3/1/2012): <http://www.livingreviews.org/lrr-2008-9>
- [4] Abdo, A. A., et al., “A limit on the variation of the speed of light arising from quantum gravity effects”, *Nature*, vol. 462, pp. 331–334, Nov. 2009.
- [5] Taylor, A. M., Vovk, I., Neronov, A., ”Extragalactic magnetic fields constraints from simultaneous GeV-TeV observations of blazars”, *Astronomy and Astrophysics*, vol. 529, pp. 144, May 2011.
- [6] Broderick, A. E., Chang, P., & Pfrommer, C., “The Cosmological Impact of Luminous TeV Blazars. I. Implications of Plasma Instabilities for the Intergalactic Magnetic Field and Extragalactic Gamma-Ray Background”, *ApJ*, vol. 752, pp. 22, June 2012
- [7] Fields, B. D., Sarkar, S., et al., “Big Bang Nucleosynthesis”, in: “Review of Particle Physics”, *The Particle Data Group*, vol. 86, pp. 275-288, July 2012.
- [8] Fan, X., Carilli, C. L., & Keating, B., “Observational Constraints on Cosmic Reionization”, *ARA&A*, vol. 44, pp. 415–462, Sept. 2006.
- [9] Yao, Y., et al., “Detecting the Warm-Hot Intergalactic Medium through X-Ray Absorption Lines”, *ApJ*, vol. 746, pp. 166, Feb. 2012.
- [10] Meyer, M., et al., “Limits on the extragalactic background light in the Fermi era”, *A&A*, vol. 542, pp. A59–A72, June 2012.
- [11] Laing, R. A., & Bridle, A. H., “Rotation measure variation across M84”, *MNRAS*, vol. 228, pp. 557–571, Oct. 1987.
- [12] Finogunov, A. et al, 2008, *ApJ*, 696, 911.

- [13] della Ceca, R., et al., “The properties of X-ray selected active galactic nuclei. 3: The radio-quiet versus radio-loud samples”, *ApJ*, vol. 430, pp. 533–544, Aug. 1994.
- [14] Kellermann, K. I., et al., “Sub-Milliarcsecond Imaging of Quasars and Active Galactic Nuclei”, *AJ*, vol. 115, pp. 1295–1318, April 1998.
- [15] Marshall, H. L., et al., “A High-Resolution X-Ray Image of the Jet in M87”, *ApJ*, vol. 564, pp. 683–687, Jan. 2002.
- [16] Hardcastle, M. J., et al., “New Results on Particle Acceleration in the Centaurus A Jet and Counterjet from a Deep Chandra Observation”, *ApJL*, vol. 670, pp. L81–L84, Dec. 2007.
- [17] Curtis, H. D., “Descriptions of 762 Nebulae and Clusters Photographed with the Crossley Reflector”, *Publications of Lick Observatory*, vol. 13, pp. 9–42, 1918.
- [18] Schmidt, M., “3C 273 : A Star-Like Object with Large Red-Shift”, *Nature*, vol. 197, pp. 1040, March 1963.
- [19] Tavecchio, F., et al., “The X-Ray Jet of PKS 0637-752: Inverse Compton Radiation from the Cosmic Microwave Background?”, *ApJL*, vol. 544, pp. L23–L26, Nov. 2000.
- [20] T. Savolainen, *et. al.*, “Relativistic beaming and gamma-ray brightness of blazars”, *A&A*, vol. 512, pp. 24-30, Jan. 2010.
- [21] Harris, D. E., & Krawczynski, H., “X-Ray Emission from Extragalactic Jets”, *ARA&A*, vol. 44, pp. 463–506, Sept. 2006.
- [22] Harris, D. E., & Krawczynski, H., “X-Ray Emission Processes in Radio Jets”, *ApJ*, vol. 565, pp. 244–255, Jan. 2002.
- [23] Atoyan, A., & Dermer, C. D., “Synchrotron versus Compton Interpretations for Extended X-Ray Jets”, *ApJ*, vol. 613, pp. 151–158, Sept. 2004.
- [24] Abdo, A. A., et al., “Fermi Gamma-Ray Imaging of a Radio Galaxy”, *Science*, vol. 328, pp. 725, May 2010.
- [25] Yang, R.-Z., et al., “Deep observation of the giant radio lobes of Centaurus A with the Fermi Large Area Telescope”, *A&A*, vol. 542, pp. A19. June 2012.
- [26] Cheung, C. C., “Radio Identification of the X-Ray Jet in the $z=4.3$ Quasar GB 1508+5714”, *ApJL*, vol. 600, pp. L23–L26, Jan. 2004.
- [27] Sikora, M., & Madejski, G., “On Pair Content and Variability of Subparsec Jets in Quasars”, *ApJ*, vol. 534, pp. 109–113, May 2000.
- [28] Celotti, A., & Fabian, A. C., “The Kinetic Power and Luminosity of Parsecscale Radio Jets - an Argument for Heavy Jets”, *MNRAS*, vol. 264, pp. 228, Sept. 1993.

- [29] Ghisellini, G., “Electron-positron pairs in blazar jets and γ -ray loud radio galaxies”, *MNRAS*, vol. 424, pp. L26–L30, July 2012.
- [30] Boehringer, H., et al., “A ROSAT HRI study of the interaction of the X-ray-emitting gas and radio lobes of NGC 1275”, *MNRAS*, vol. 264, pp. L25–L28, Oct. 1993.
- [31] Carilli, C. L., Perley, R. A., & Harris, D. E., “Observations of Interaction Between Cluster Gas and the Radio Lobes of Cygnus-A”, *MNRAS*, vol. 270, pp. 173, Sept. 1994.
- [32] Fabian, A. C., et al., “A very deep Chandra observation of the Perseus cluster: shocks, ripples and conduction”, *MNRAS*, vol. 366, pp. 417–428, Feb. 2006.
- [33] McNamara, B. R., & Nulsen, P. E. J., “Mechanical feedback from active galactic nuclei in galaxies, groups and clusters”, *New Journal of Physics*, vol. 14, pp. 055023, May 2012.
- [34] Bîrzan, L., et al., “Radiative Efficiency and Content of Extragalactic Radio Sources: Toward a Universal Scaling Relation between Jet Power and Radio Power”, *ApJ*, vol. 686, pp. 859–880, Oct. 2008.
- [35] Rees, M. J., “New Interpretation of Extragalactic Radio Sources”, *Nature*, vol. 229, pp. 312–317, Jan. 1971.
- [36] Longair, M. S., Ryle, M., & Scheuer, P. A. G., “Models of extended radiosources”, *MNRAS*, vol. 164, pp. 243, 1973.
- [37] Scheuer, P. A. G., “Models of extragalactic radio sources with a continuous energy supply from a central object”, *MNRAS*, vol. 166, pp. 513–528, March 1974.
- [38] Blandford, R. D., & Rees, M. J., “A ‘twin-exhaust’ model for double radio sources”, *MNRAS*, vol. 169, pp. 395–415, Dec. 1974.
- [39] Aloy, M. A., Mimica, P., 2012, “Simulations of Jets from Active Galactic Nuclei and Gamma Ray Bursts”, in: “Relativistic Jets from Active Galactic Nuclei”, Eds. M. Boettcher, D. E. Harris, H. Krawczynski, Wiley-VCH, pp. 297–340, Feb. 2012.
- [40] McKinney, J. C., Tchekhovskoy, A., & Blandford, R. D., “General relativistic magnetohydrodynamic simulations of magnetically choked accretion flows around black holes”, *MNRAS*, vol. 423, pp. 3083–3117, July 2012.
- [41] McKinney, J. C., & Blandford, R. D., “Stability of relativistic jets from rotating, accreting black holes via fully three-dimensional magnetohydrodynamic simulations”, *MNRAS*, vol. 394, pp. L126–L130, March 2009.
- [42] Sironi, L., & Spitkovsky, A., “Particle Acceleration in Relativistic Magnetized Collisionless Electron-Ion Shocks”, *ApJ*, vol. 726, pp. 75, Jan. 2011.

- [43] Urry, C. M., Padovani, P., “Unified Schemes for Radio-Loud Active Galactic Nuclei”, *Astronomical Society of the Pacific*, vol. 107, pp. 803–845, Sept. 1995.
- [44] Czerny, B., & Elvis, M., “Constraints on quasar accretion disks from the optical/ultraviolet/soft X-ray big bump”, *ApJ*, vol. 321, pp. 305–320, Oct. 1987.
- [45] Koratkar, A., & Blaes, O., “The Ultraviolet and Optical Continuum Emission in Active Galactic Nuclei: The Status of Accretion Disks”, *Astronomical Society of the Pacific*, vol. 111, pp. 1–30, Jan. 1999.
- [46] Ichimaru, S., “Bimodal behavior of accretion disks - Theory and application to Cygnus X-1 transitions”, *ApJ*, vol. 214, pp. 840–855, June 1977.
- [47] Narayan, R., et al., “The Magnetohydrodynamics of Convection-dominated Accretion Flows”, *ApJ*, vol. 577, pp. 295–301, Sept. 2002.
- [48] Henri, G., & Petrucci, P. O., “Anisotropic illumination of AGN’s accretion disk by a non thermal source. I. General theory and application to the Newtonian geometry.”, *A&A*, vol. 326, pp. 87–98, Oct. 1997.
- [49] Malzac, J., et al., “Anisotropic illumination in AGNs. The reflected component. Comparison to hard X-ray spectra from Seyfert Galaxies”, *A&A*, vol. 336, pp. 807–814, Aug. 1998.
- [50] Galeev, A. A., Rosner, R., & Vaiana, G. S., “Structured coronae of accretion disks”, *ApJ*, vol. 229, pp. 318–326, April 1979.
- [51] Fabian, A. C., et al., “X-ray fluorescence from the inner disc in Cygnus X-1”, *MNRAS*, vol. 238, pp. 729–736, May 1989.
- [52] Reynolds, C. S., & Nowak, M. A., “Fluorescent iron lines as a probe of astrophysical black hole systems”, *PhysRep*, vol. 377, pp. 389–466, April 2003.
- [53] Ross, R. R., & Fabian, A. C., “A comprehensive range of X-ray ionized-reflection models”, *MNRAS*, vol. 358, pp. 211–216, 3/2005.
- [54] Ross, R. R., & Fabian, A. C., “X-ray reflection in accreting stellar-mass black hole systems”, *MNRAS*, vol. 381, pp. 1697–1701, Nov. 2007.
- [55] Brenneman, L. W., & Reynolds, C. S., “Constraining Black Hole Spin via X-Ray Spectroscopy”, *ApJ*, vol. 652, pp. 1028–1043, Dec. 2006.
- [56] Doeleman, S. S., et al., “Event-horizon-scale structure in the supermassive black hole candidate at the Galactic Centre”, *Nature*, vol. 455, pp. 78–80, Sept. 2008.
- [57] Véron-Cetty, M. P., & Véron, P., “The emission line spectrum of active galactic nuclei and the unifying scheme”, *A&ARv*, vol. 10, pp. 81–133, 2000.

- [58] Peterson, B. M., “The Masses of Black Holes in Active Galactic Nuclei”, *The Central Engine of Active Galactic Nuclei*, vol. 373, p. 3, Oct. 2007.
- [59] Kaspi, S., “Advances in Reverberation Mapping”, *The Central Engine of Active Galactic Nuclei*, vol. 373, p. 13, Oct. 2007.
- [60] Rawlings, S., & Saunders, R., “Evidence for a common central-engine mechanism in all extragalactic radio sources”, *Nature*, vol. 349, pp. 138–140, Jan. 1991.
- [61] Celotti, A., et al., “Jets and accretion processes in active galactic nuclei: further clues”, *MNRAS*, vol. 286, pp. 415–424, April 1997.
- [62] Maraschi, L., & Tavecchio, F., “The Jet-Disk Connection and Blazar Unification”, *ApJ*, vol. 593, pp. 667–675, Aug. 2003.
- [63] Kawakatu, N., Nagao, T., & Woo, J.-H., “Exploring the Disk-Jet Connection from the Properties of Narrow-Line Regions in Powerful Young Radio-Loud Active Galactic Nuclei”, *ApJ*, vol. 693, pp. 1686–1695, March 2009.
- [64] Elitzur, M., “Unification Issues and the AGN Torus”, *The Central Engine of Active Galactic Nuclei*, vol. 373, pp. 415, Oct. 2007.
- [65] Nenkova, M., et al., “AGN Dusty Tori. I. Handling of Clumpy Media”, *ApJ*, vol. 685, pp. 147–159, 160-, Sept. 2008, “AGN Dusty Tori. II. Observational Implications of Clumpiness”, *ApJ*, vol. 685, pp. 160–180, Sept. 2008.
- [66] Chelouche, D., “AGN Outflows: Observations and Their Interpretation”, *The Central Engine of Active Galactic Nuclei*, vol. 373, pp. 277, Oct. 2007.
- [67] Stickel, M., et al., “The complete sample of 1 Jansky BL Lacertae objects. I - Summary properties”, *ApJ*, vol. 374, pp. 431–439, June 1991.
- [68] Stocke, J. T., et al., “The Einstein Observatory Extended Medium-Sensitivity Survey. II - The optical identifications”, *ApJS*, vol. 76, pp. 813–874, July 1991.
- [69] Ghisellini, G., et al., “The transition between BL Lac objects and flat spectrum radio quasars”, *MNRAS*, vol. 414, pp. 2674–2689, July 2011.
- [70] Giommi, P., et al., “A simplified view of blazars: clearing the fog around long-standing selection effects”, *MNRAS*, vol. 420, pp. 2899–2911, March 2012.
- [71] Atwood, W. B., et al., “The Large Area Telescope on the Fermi Gamma-Ray Space Telescope Mission”, *ApJ*, vol. 697, pp. 1071–1102, June 2009.
- [72] Aharonian, F., et al., “High energy astrophysics with ground-based gamma ray detectors”, *Reports on Progress in Physics*, vol. 71, pp. 096901, Sept. 2008.

- [73] Abdo, A. A., et al., “Fermi Large Area Telescope Observations of Markarian 421: The Missing Piece of its Spectral Energy Distribution”, *ApJ*, vol. 736, pp. 131, August 2011.
- [74] Abdo, A. A., et al., “Insights into the High-energy γ -ray Emission of Markarian 501 from Extensive Multifrequency Observations in the Fermi Era”, *ApJ*, vol. 727, pp. 129, Feb. 2011.
- [75] Nolan, P. L., et al., “Fermi Large Area Telescope Second Source Catalog”, *ApJS*, vol. 199, pp. 31– April 2012.
- [76] Ajello, M., et al., “The Luminosity Function of Fermi-detected Flat-spectrum Radio Quasars”, *ApJ*, vol. 751, pp. 108–128, June 2012.
- [77] Fossati, G., et al., “A unifying view of the spectral energy distributions of blazars”, *MNRAS*, vol. 299, pp. 433–448, Sept. 1998.
- [78] Ghisellini, G., et al., “A theoretical unifying scheme for gamma-ray bright blazars”, *MNRAS*, vol. 301, pp. 451–468, Dec. 1998.
- [79] Krawczynski, H., et al., “Simultaneous X-Ray and TeV Gamma-Ray Observation of the TeV Blazar Markarian 421 during 2000 February and May”, *ApJ*, vol. 559, pp. 187–195, Sept. 2001.
- [80] Konopelko, A., et al., “Modeling the TeV Gamma-Ray Spectra of Two Low-Redshift Active Galactic Nuclei: Markarian 501 and Markarian 421”, *ApJ*, vol. 597, pp. 851–859, Nov. 2003.
- [81] Gaidos, J. A., et al., “Extremely rapid bursts of TeV photons from the active galaxy Markarian 421”, *Nature*, vol. 383, pp. 319–320, Sept. 1996.
- [82] Aharonian, F., et al., “An Exceptional Very High Energy Gamma-Ray Flare of PKS 2155-304”, *ApJL*, vol. 664, pp. L71–L74, Aug. 2007.
- [83] Albert, J., et al., “Variable Very High Energy γ -Ray Emission from Markarian 501”, *ApJ*, vol. 669, pp. 862–883, Nov. 2007.
- [84] Begelman, M. C., Fabian, A. C., & Rees, M. J., “Implications of very rapid TeV variability in blazars”, *MNRAS*, vol. 384, pp. L19–L23, Feb. 2008.
- [85] Acciari, V. A., et al., “TeV and Multi-wavelength Observations of Mrk 421 in 2006-2008”, *ApJ*, vol. 738, pp. 25, Sept. 2011.
- [86] Aleksić, J., et al., “Discovery of VHE γ -rays from the blazar 1ES 1215+303 with the MAGIC telescopes and simultaneous multi-wavelength observations”, *A&A*, vol. 544, pp. A142– Aug. 2012.
- [87] Krawczynski, H., et al., “Multiwavelength Observations of Strong Flares from the TeV Blazar 1ES 1959+650”, *ApJ*, vol. 601, pp. 151–164, Jan. 2004.

- [88] H.E.S.S. Collaboration, et al., “A multiwavelength view of the flaring state of PKS 2155-304 in 2006”, *A&A*, vol. 539, pp. A149–, March 2012.
- [89] Georganopoulos, M., & Kazanas, D., “Decelerating flows in TeV blazars”, *New Astronomy Reviews*, vol. 48, pp. 403–405, Apr. 2004.
- [90] Ghisellini, G., Tavecchio, F., & Chiaberge, M., “Structured jets in TeV BL Lac objects and radiogalaxies. Implications for the observed properties”, *A&A*, vol. 432, pp. 401–410, 3/2005.
- [91] Abdo, A. A., et al., “The Spectral Energy Distribution of Fermi Bright Blazars”, *ApJ*, vol. 716, pp. 30–70, June 2010.
- [92] Giommi, P., et al., “Simultaneous Planck, Swift, and Fermi observations of X-ray and γ -ray selected blazars”, *A&A*, vol. 541, pp. A160, May 2012.
- [93] Fossati, G., et al., “Multiwavelength Observations of Markarian 421 in 2001 March: An Unprecedented View on the X-Ray/TeV Correlated Variability”, *ApJ*, vol. 677, pp. 906–925, April 2008.
- [94] Ghirlanda, G., et al., “The radio- γ -ray connection in Fermi blazars”, *MNRAS*, vol. 413, pp. 852–862, May 2011.
- [95] Ackermann, M., et al., “The Radio/Gamma-Ray Connection in Active Galactic Nuclei in the Era of the Fermi Large Area Telescope”, *ApJ*, vol. 741, pp. 30, Nov. 2011.
- [96] Nieppola, E., et al., “Correlation between Fermi/LAT gamma-ray and 37 GHz radio properties of northern AGN averaged over 11 months”, *A&A*, vol. 535, pp. A69, Nov. 2011.
- [97] Krawczynski, H., et al., “X-ray/TeV-gamma-ray observations of several strong flares of Mkn 501 during 1997 and implications”, *A&A*, vol. 353, pp. 97–107, Jan. 2000.
- [98] Marscher, A. P., et al., “The inner jet of an active galactic nucleus as revealed by a radio-to- γ -ray outburst”, *Nature*, vol. 452, pp. 966–969, April 2008.
- [99] Abdo, A. A., et al., “A change in the optical polarization associated with a γ -ray flare in the blazar 3C279”, *Nature*, vol. 463, pp. 919–923, Feb. 2010.
- [100] Kirk, J. G., & Mastichiadis, A., “Variability patterns of synchrotron and inverse Compton emission in blazars”, *Astroparticle Physics*, vol. 11, pp. 45–48, June 1999.
- [101] Takahashi, T., et al., “Complex Spectral Variability from Intensive Multiwavelength Monitoring of Markarian 421 in 1998”, *ApJL*, vol. 542, pp. L105–L109, Oct. 2000.
- [102] Garson, A. B., III, Baring, M. G., & Krawczynski, H., “A Suzaku X-ray Study of the Particle Acceleration Processes in the Relativistic Jet of Blazar Mrk 421”, *ApJ*, vol. 722, pp. 358–366, Oct. 2010.

- [103] Mannheim, K., “The proton blazar”, *A&A*, vol. 269, pp. 67–76, March 1993.
- [104] Mücke, A., et al., “BL Lac objects in the synchrotron proton blazar model”, *Astroparticle Physics*, vol. 18, pp. 593–613, March 2003.
- [105] Aharonian, F. A., “TeV gamma rays from BL Lac objects due to synchrotron radiation of extremely high energy protons”, *New Astronomy*, vol. 5, pp. 377–395, Nov. 2000.
- [106] Reimer, A., “On the Physics of Hadronic Blazar Emission Models”, *Journal of Physics Conference Series*, vol. 355, pp. 012011– March 2012.
- [107] Boettcher, M., “Modeling the Spectral Energy Distributions and Variability of Blazars”, [arXiv:1205.0539], March 2012.
- [108] Hopkins, P. F., “Dynamical delays between starburst and AGN activity in galaxy nuclei”, *MNRAS*, vol. 420, pp. L8–L12, Feb. 2012.
- [109] Shakura, N. I., & Sunyaev, R. A., “Black holes in binary systems. Observational appearance.”, *A&A*, vol. 24, pp. 337–355, 1973.
- [110] Page, D. N., & Thorne, K. S., “Disk-Accretion onto a Black Hole. Time-Averaged Structure of Accretion Disk”, *ApJ*, vol. 191, pp. 499–506, July 1974.
- [111] Balbus, S. A., & Hawley, J. F., “A powerful local shear instability in weakly magnetized disks. I - Linear analysis. II - Nonlinear evolution”, *ApJ*, vol. 376, pp. 214–233, July 1991.
- [112] Narayan, R., & Yi, I., “Advection-dominated accretion: A self-similar solution”, *ApJL*, vol. 428, pp. L13–L16, June 1994.
- [113] Narayan, R., Igumenshchev, I. V., & Abramowicz, M. A., “Self-similar Accretion Flows with Convection”, *ApJ*, vol. 539, pp. 798–808, Aug. 2000.
- [114] Quataert, E., & Gruzinov, A., “Convection-dominated Accretion Flows”, *ApJ*, vol. 539, pp. 809–814, Aug. 2000.
- [115] Blandford, R. D., & Begelman, M. C., “On the fate of gas accreting at a low rate on to a black hole”, *MNRAS*, vol. 303, pp. L1–L5, Feb. 1999.
- [116] Begelman, M. C., “Radiatively inefficient accretion: breezes, winds and hyperaccretion”, *MNRAS*, vol. 420, pp. 2912–2923, March 2012.
- [117] Blandford, R. D., & Znajek, R. L., “Electromagnetic extraction of energy from Kerr black holes”, *MNRAS*, vol. 179, pp. 433–456, May 1977.
- [118] Noble, S. C., et al., “Radiative Efficiency and Thermal Spectrum of Accretion onto Schwarzschild Black Holes”, *ApJ*, vol. 743, pp. 115, Dec. 2011.

- [119] Penna, R. F., Sä Dowski, A., & McKinney, J. C., “Thin-disc theory with a non-zero-torque boundary condition and comparisons with simulations”, *MNRAS*, vol. 420, pp. 684–698, Feb. 2012.
- [120] McKinney, J. C., & Narayan, R., “Disc-jet coupling in black hole accretion systems - I. General relativistic magnetohydrodynamical models”, *MNRAS*, vol. 375, pp. 513–530, Feb. 2007.
- [121] Beckwith, K., et al., “The Influence of Magnetic Field Geometry on the Evolution of Black Hole Accretion Flows: Similar Disks, Drastically Different Jets”, *ApJ*, vol. 678, pp. 1180–1199, May 2008.
- [122] Rees, M., “Structure and properties of nearby galaxies”, *Proceedings of the symposium, bad Muen- stereifel, West Germany*, vol. 1, no. 1, pp. 237–244, 1978.
- [123] Volonteri, M., “Formation of supermassive black holes”, *A&ARv*, vol. 18, pp. 279–315, July 2010.
- [124] Willott, C., et al., “Eddington-limited Accretion and the Black Hole Mass Function at Redshift 6”, *AJ*, vol. 140, pp. 546–560, Aug. 2010.
- [125] Mortlock, D., et al., “A luminous quasar at a redshift of $z=7.085$ ”, *Nature.*, vol. 474, pp. 616–619, June 2011
- [126] Bromm, V., et al., “Formation of the First Supermassive Black Holes”, *ApJ*, vol. 596, pp. 34–46, Oct. 2003.
- [127] Devecchi, B. & Volonteri, M., “Formation of the First Nuclear Clusters and Massive Black Holes at High Redshift”, *ApJ*, vol. 694, pp. 302–313, Mar. 2009.
- [128] Lynden-Bell, D., “Galactic Nuclei as Collapsed Old Quasars”, *Nature*, vol. 223, pp. 690–694, Aug. 1969.
- [129] Soltan, A., “Masses of quasars”, *MNRAS*, vol. 200, pp. 115–122, July 1982.
- [130] Treister, E. et al., “Major Galaxy Mergers and the Growth of Supermassive Black Holes in Quasars”, *Science*, vol. 328, pp. 600–, Apr. 2010.
- [131] Hopkins, P. F. and Hernquist, L., “Fueling Low-Level AGN Activity through Stochastic Accretion of Cold Gas”, *ApJS*, vol. 166, pp. 1–36, Sept. 2006.
- [132] Antonucci, R., “Unified models for active galactic nuclei and quasars”, *ARA&A*, vol. 31, pp. 473–521, 1993.
- [133] Lawrence, A., “The relative frequency of broad-lined and narrow-lined active galactic nuclei - Implications for unified schemes”, *MNRAS*, vol. 252, pp. 586–592, Oct. 1991.

- [134] Treister, E. and Urry, C. M., “The Evolution of Obscuration in Active Galactic Nuclei”, *ApJL*, vol. 652, pp. L79–L82, Dec. 2006.
- [135] Hickox, R. C. & Markevitch, M., “Absolute Measurement of the Unresolved Cosmic X-Ray Background in the 0.5-8 keV Band with Chandra”, *ApJ*, vol. 645, pp. 95–114, July 2006.
- [136] Mushotzky, R., et al., “Resolving the extragalactic hard X-ray background”, *Nature*, vol. 404, pp. 459–464, Mar. 2000.
- [137] Setti, G., & Woltjer, L., “Active Galactic Nuclei and the spectrum of the X-ray background”, *A&A*, vol. 224, pp. L21–L23, Oct. 1989.
- [138] Treister, E. et al “The Space Density of Compton Thick AGN and the X-ray Background”, *ApJ*, vol. 696, pp. 110–120, May 2009.
- [139] Draper, A. R., & Ballantyne, D. R., “Balancing the Cosmic Energy Budget: The Cosmic X-ray Background, Blazars, and the Compton Thick Active Galactic Nucleus Fraction”, *ApJ*, vol. 707, pp. 778–786, Dec. 2009.
- [140] Burlon, D., et al., “Three-year Swift-BAT Survey of Active Galactic Nuclei: Reconciling Theory and Observations?”, *ApJ*, vol. 728, pp. 58–+, Feb. 2011.
- [141] Treister, E., & Urry, C. M., “Active Galactic Nuclei Unification and the X-Ray Background”, *ApJ*, vol. 630, pp. 115–121, Sept. 2005.
- [142] Gilli, R. et al., “The synthesis of the cosmic X-ray background in the Chandra and XMM-Newton era”, *A&A*, vol. 463, pp. 79–96, Feb. 2007.
- [143] Salucci, P. et al. “Mass function of dormant black holes and the evolution of active galactic nuclei”, *MNRAS*, vol. 307, pp. 637–644, Aug. 1999.
- [144] Yu, Q. and S. Tremaine, “Observational constraints on growth of massive black holes”, *MNRAS*, vol. 335, pp. 965–976, Oct. 2002.
- [145] Marconi, A. et al, “Local supermassive black holes, relics of active galactic nuclei and the X-ray background”, *MNRAS*, vol. 351, pp. 169–185, June 2004.
- [146] Shankar, F., et al., “Supermassive black hole demography: the match between the local and accreted mass functions”, *MNRAS*, vol. 354, pp. 1020–1030, Nov. 2004.
- [147] Natarajan, P., & Treister, E., “Is there an upper limit to black hole masses?”, *MNRAS*, vol. 393, pp. 838–845, Mar. 2009.
- [148] Shankar, F., et al., “Self-Consistent Models of the AGN and Black Hole Populations: Duty Cycles, Accretion Rates, and the Mean Radiative Efficiency”, *ApJ*, vol. 690, pp. 20–41, Jan. 2009.

- [149] Treister, E., et al., “Black hole growth in the early Universe is self-regulated and largely hidden from view.”, *Nature*, vol. 474, pp. 356–358, 2011.
- [150] L. L. Cowie, A. J. Barger, and G. Hasinger, “The faintest X-ray sources from $z=0-8$,” *ArXiv e-prints*, Oct. 2011.
- [151] C. J. Willott, “No Evidence of Obscured, Accreting Black Holes in Most $z = 6$ Star-forming Galaxies,” *ApJL*, vol. 742, p. L8, Nov. 2011.
- [152] Volonteri, M., Haardt, F., & Madau, P., “The Assembly and Merging History of Supermassive Black Holes in Hierarchical Models of Galaxy Formation”, *ApJ*, vol. 582, pp. 559–573, Jan. 2003.
- [153] M. Volonteri and N. Y. Gnedin, “Relative Role of Stars and Quasars in Cosmic Reionization,” *ApJ*, vol. 703, pp. 2113–2117, Oct. 2009.
- [154] Volonteri, M., & Begelman, M. C., “Quasi-stars and the cosmic evolution of massive black holes”, *MNRAS*, vol. 409, pp. 1022–1032, Dec. 2010.
- [155] Natarajan, P., “The formation and evolution of massive black hole seeds in the early Universe”, *Bulletin of the Astronomical Society of India*, vol. 39, pp. 145–161, Mar. 2011.
- [156] Di Matteo, T. et al., “Energy input from quasars regulates the growth and activity of black holes and their host galaxies”, *Nature*, vol. 433, pp.604–607, Feb. 2005
- [157] Barnes, J. E., & Hernquist, L. E., “Fueling starburst galaxies with gas-rich mergers”, *ApJL*, vol. 370, pp. L65–L68, 4/1991.
- [158] Sanders, D. et al., “Ultraluminous infrared galaxies and the origin of quasars”, *ApJ*, vol. 325, pp. 74–91, Feb. 1988.
- [159] De Robertis, M. M., Yee, H. K. C., & Hayhoe, K., “A CCD Study of the Environment of Seyfert Galaxies. II. Testing the Interaction Hypothesis”, *ApJ*, vol. 496, pp. 93, March 1998.
- [160] Moore, B., et al., “Galaxy harassment and the evolution of clusters of galaxies”, *Nature*, vol.379, pp.613-616, Feb. 1996
- [161] Kormendy, J. and Kennicutt, C., Jr., “Secular Evolution and the Formation of Pseudobulges in Disk Galaxies”, *ARA&A*, vol. 42, pp.603–683, Sep. 2004
- [162] Finn, R., et al., “WFPC2 Imaging of Quasar Environments: A Comparison of Large Bright Quasar Survey and Hubble Space Telescope Archive Quasars” *ApJ*, vol. 557, pp.578–593, Aug. 2001
- [163] Hopkins, P., and Hernquist, L., “A Characteristic Division Between the Fueling of Quasars and Seyferts: Five Simple Tests”, *ApJ*, vol.694, pp.599–609, March 2009.

- [164] Treister, E., et al., “Major Galaxy Mergers Only Trigger the Most Luminous Active Galactic Nuclei”, *ApJL*, vol.758, pp.L39, Oct. 2012
- [165] Darg, D., et al., Galaxy Zoo: the properties of merging galaxies in the nearby Universe ? local environments, colours, masses, star formation rates and AGN activity”, *MNRAS*, vol. 401, pp.1552–1563, Jan. 2010
- [166] Aird, J., et al., “The evolution of the hard X-ray luminosity function of AGN”, *MNRAS*, vol. 401, pp. 2531–2551, Feb. 2010.
- [167] Ueda, Y., et al. “Cosmological Evolution of the Hard X-Ray Active Galactic Nucleus Luminosity Function and the Origin of the Hard X-Ray Background”, *ApJ*, vol. 598, pp. 886–908, Dec. 2003.
- [168] Kauffmann, G., & Haehnelt, M., “A unified model for the evolution of galaxies and quasars”, *MNRAS*, vol.311, pp.576–588, Jan. 2000
- [169] Dahlen, T., et al., “Evolution of the Luminosity Function, Star Formation Rate, Morphology, and Size of Star-forming Galaxies Selected at Rest-Frame 1500 and 2800 Å”, *ApJ*, vol. 654, pp. 172–185, Jan. 2007.
- [170] Cisternas, M., et al., “The Bulk of the Black Hole Growth Since $z = 1$ Occurs in a Secular Universe: No Major Merger-AGN Connection”, *ApJ*, vol.726, pp.57, Jan. 2011
- [171] Schawinski, K., et al., “HST WFC3/IR Observations of Active Galactic Nucleus Host Galaxies at $z = 2$: Supermassive Black Holes Grow in Disk Galaxies”, *ApJL*, vol.727, pp.L31, Feb. 2011
- [172] Kocevski, D., et al., “CANDELS: Constraining the AGN-Merger Connection with Host Morphologies at $z = 2$ ”, vol.744, pp.148, Jan. 2012
- [173] Yao, L., et al., “CO Molecular Gas in Infrared-luminous Galaxies”, *ApJ*, vol. 588, pp. 771–791, May 2003.
- [174] E. Treister, C. M. Urry, K. Schawinski, C. N. Cardamone, and D. B. Sanders, “Heavily Obscured Active Galactic Nuclei in High-redshift Luminous Infrared Galaxies,” *ApJL*, vol. 722, pp. L238–L243, Oct. 2010.
- [175] Doleman, S., “Building an event horizon telescope: (sub)mm VLBI in the ALMA era”, Proceedings of the 10th European VLBI Network Symposium and EVN Users Meeting: VLBI and the new generation of radio arrays. September 20-24, 2010. Manchester, UK. Published online at <http://pos.sissa.it/cgi-bin/reader/conf.cgi?confid=125>, id.53, 2010.
- [176] Ballantyne, D., et al., “Lifting the Veil on Obscured Accretion: Active Galactic Nuclei Number Counts and Survey Strategies for Imaging Hard X-Ray Missions”, *ApJ*, vol. 736, pp. 56–+, July 2011.

- [177] Takahashi, T., et al., “The ASTRO-H Mission”, in *Society of Photo-Optical Instrumentation Engineers (SPIE) Conference Series*, of *Society of Photo-Optical Instrumentation Engineers (SPIE) Conference Series*, vol. 7732, pp. 77320Z-77320Z-18, July 2010.
- [178] Beilicke, M., et al., “Design and tests of the hard x-ray polarimeter X-Calibur”, *SPIE Proceedings*, vol. 8145, pp. 240, Sep. 2011.
- [179] Pearce, M., et al., “Balloon-borne gamma-ray polarimetry”, Presented at 20th ESA Symposium on European Rocket and Balloon Programs and Related Research, Hyères, 22-26 May, 2011 [arXiv:1106.1322].
- [180] Krawczynski, H., “The Polarization Properties of Inverse Compton Emission and Implications for Blazar Observations with the GEMS X-Ray Polarimeter”, *ApJ*, vol. 744, pp. 30, Jan. 2012.
- [181] Gair, J. R., et al., “Constraining properties of the black hole population using LISA”, *Classical and Quantum Gravity*, vol. 28, pp. 094018, May 2011.
- [182] Barcons, X., “Probing the growth of supermassive black holes at high redshift with IXO”, 38th COSPAR Scientific Assembly, vol. 38, pp. 2359, 2010.
- [183] Black, J., et al., “The GEMS photoelectric x-ray polarimeters”, vol. 7732, pp. 77320X-77320X-11, July 2010.
- [184] Actis, M., et al., “Design concepts for the Cherenkov Telescope Array CTA: an advanced facility for ground-based high-energy gamma-ray astronomy”, *Experimental Astronomy*, vol. 32, pp. 193–316, Dec. 2011.